

COLUMN ABUNDANCES OF CARBON
DIOXIDE AND METHANE RETRIEVED
FROM GROUND-BASED NEAR-INFRARED
SOLAR SPECTRA

Thesis by

Rebecca A. Washenfelder

In Partial Fulfillment of the Requirements for the
Degree of

Doctor of Philosophy

CALIFORNIA INSTITUTE OF TECHNOLOGY

Pasadena, California

2006

(Defended May 22, 2006)

© 2006

Rebecca A. Washenfelder

All Rights Reserved

Acknowledgements

Most importantly, I thank my advisor, Paul Wennberg, who welcomed me to Caltech. I truly appreciate his guidance, and I am continually inspired by his clear insight into scientific problems. As a member of Paul's group, I have enjoyed the opportunity to work on exciting research projects and travel throughout the world. In addition to Paul, I thank my committee members, Mitchio Okumura, James Randerson, and Geoffrey Toon for keeping my Ph.D. on track and aimed toward completion.

I thank Geoffrey Toon and Jean-Francois Blavier for the enormous amount of time and energy they have invested in teaching me about Linux, Fourier Transform spectrometry, and a dozen other topics. Zhonghua Yang and Gretchen Aleks have been great friends and collaborators in this project. I thank Gretchen for adopting the Park Falls observatory and continuing this project into the future. I enjoyed assembling the second observatory and traveling to Australia with Yael Yavin. Yael's independence in assembling the third observatory with Gretchen has been invaluable in making my thesis writing possible. I appreciate the instruction I received from Dave Petterson in electronics and cable-making. I thank Norton Allen for his work in automating the Fourier Transform spectrometer data acquisition. The volley of emails between Jean-Francois Blavier and Norton Allen has been educational, even if I couldn't always keep up.

Caltech has been an accommodating place for instrumental work. I thank Mark Harriman and the Athletic Center staff for providing space for the observatories. It was pleasant to spend so many hours near the swimming pool. Among the many people on campus who helped with this project, I would particularly like to thank Rick Gerhart from the Glassblowing Shop, Rick Germond from the Central Warehouse, Corey Campbell and Moses from the Main Stockroom, and Mike Anchondo from the Electrical Shop. I thank the Physics Machine Shop staff, especially Armando De Las Casas and Rick Paniagua who guided me during the many happy hours I spent there. Leticia Calderon and Irma Black have smoothed the way administratively whenever there has been trouble. Thanks to

Michael Black, David Kewley, and Scott Dungan for setting up the RAID and solving my computer troubles.

Beyond Caltech, I have enjoyed my ongoing collaboration with Nick Deutscher, David Griffith, and Glenn Bryant at the University of Wollongong, and with Brian Connor and Vanessa Sherlock at NIWA. Thanks to Ankur Desai, Dan Ricciuto, and Ken Davis at Pennsylvania State University for sharing their data and answering my many questions about eddy covariance measurements. Thanks to Linda Brown for her insight into laboratory spectroscopy. Finally, I would like to thank Ross Salawitch, Charles Miller, David Crisp, and the OCO science team.

I have thoroughly enjoyed my time in the Wennberg group with Karena McKinney, Suresh Dhaniyala, Coleen Roehl, Zhonghua Yang, Julie Fry, John Crouse, Alan Kwan, Yael Yavin, Gretchen Aleks, and David McCabe. I will miss our lunch routine at the South Lake Italian Kitchen. My first year of coursework at Caltech was vastly improved by friendships with Lisa Welp, Megan Ferguson, Jamie Lindfors, and Jeff Mendez. I have enjoyed many subsequent adventures hiking, canyoneering, and cycling with Lisa and Megan.

At Pomona College, I was lucky to have professors who believed in me and gave me useful career advice, especially Professor Daniel O'Leary. Finally, I thank my family for their love and support.

Abstract

To predict future climate change, we must accurately predict future atmospheric concentrations of CO₂ and CH₄. The current budget has typically been inferred from top-down analyses of measurements from a global network of surface sites. These measurements are highly accurate, but have limited spatial coverage. In addition, accurate knowledge of local planetary boundary layer dynamics is necessary to determine fluxes.

Column measurements, defined as the vertical integral of gas concentration, can complement the existing in situ network. Because column measurements sample a larger portion of the atmosphere, they exhibit less variability than surface data, while retaining information about surface fluxes. Column measurements are not influenced by planetary boundary layer dynamics, and do not suffer from the resulting correlation between exchange and transport.

An automated observatory for measuring ground-based column abundances of CO₂, CH₄, and O₂ is described. Near-infrared spectra of the direct sun are obtained from 3,900 – 15,600 cm⁻¹ by a Bruker 125HR Fourier transform spectrometer. The observatory was assembled in Pasadena, California and then permanently deployed to Northern Wisconsin during May 2004. Under clear sky conditions, retrieved column CO₂ abundances demonstrate ~0.1% precision. Comparison of these column measurements with eight aircraft profiles of in situ CO₂ recorded during summer 2004 shows a small bias, but an excellent correlation.

The observed secular increase and seasonal amplitude of column-average CO₂ observed during the period of May 2004 – March 2006 is 1.8 ppmv yr⁻¹ and 11 ppmv, consistent with theoretical predictions that the measurements will be representative of Northern Hemisphere CO₂ exchange over seasonal timescales. Comparisons with eddy covariance measurements show that the column measurements have potential for directly observing CO₂ exchange, but that this ability is constrained by the difficulty in accounting for atmospheric transport.

Finally, the use of near-infrared spectral analysis is extended to observations of tropospheric column-average CH_4 concentrations. By employing a stratospheric “slope equilibrium” relationship between CH_4 and HF, the varying contribution of stratospheric CH_4 to the total column is inferred. This method is used to determine tropospheric column-average CH_4 VMRs from near-infrared solar absorption spectra recorded at the Kitt Peak National Solar Observatory during 1977 – 1995.

Contents

Acknowledgements	iii
Abstract	v
Contents	vii
List of Figures	xii
List of Tables	xiii
List of Abbreviations	xiv
Chapter 1 Introduction.....	1-1
1.1 The Global Carbon Budget	1-1
1.2 Remote Sensing Techniques	1-3
1.3 Outline of the Dissertation	1-5
1.4 References.....	1-6
Chapter 2 Carbon Dioxide Column Abundances at the Wisconsin Tall Tower Site	2-1
2.1 Abstract.....	2-1
2.2 Introduction.....	2-1
2.3 Instrumentation	2-3
2.3.1 Bruker 125HR Spectrometer.....	2-3
2.3.2 Laboratory and Other Instrumentation	2-5
2.3.3 Data Acquisition and Instrumental Automation.....	2-8
2.4 Measurement Site	2-9
2.5 Data Analysis.....	2-10
2.5.1 Column O ₂ and CO ₂	2-12
2.6 Comparison of FTS Column and Integrated Aircraft Profiles.....	2-17
2.6.1 Error Analysis for Column-Average CO ₂ VMR.....	2-22
2.6.2 Column-Average CO ₂ VMR During May 2004 – October 2005	2-24
2.6.3 Conclusions	2-25
2.7 Acknowledgements	2-26

2.8 References.....	2-26
Chapter 3 Surface Exchange of CO ₂ Observed by Coincident Eddy Covariance Flux and Column Measurements	
3.1 Abstract.....	3-1
3.2 Introduction.....	3-1
3.3 Column Measurements: Instrumentation and Data Analysis.....	3-4
3.4 Research Site	3-4
3.5 Seasonal CO ₂ Exchange	3-6
3.5.1 Park Falls WLEF Site During 2004 – 2005	3-6
3.5.2 Comparison to TransCom Model Predictions	3-7
3.6 Local CO ₂ Exchange	3-9
3.6.1 Bottom-Up Estimates of Local CO ₂ Exchange.....	3-9
3.6.2 Eddy Covariance: Instrumentation and Data Analysis	3-11
3.6.3 Calculation of Net Ecosystem Exchange from the Total Column.....	3-11
3.6.4 Comparison of Drawdown Observed by FTS and Eddy Covariance.....	3-15
3.7 Conclusions.....	3-18
3.8 References.....	3-19
Chapter 4 Tropospheric Methane Retrieved From Ground-Based Near-Infrared Solar Absorption Spectra	
4.1 Abstract.....	4-1
4.2 Introduction.....	4-1
4.3 Determination of Tropospheric CH ₄	4-2
4.4 The Kitt Peak Spectra.....	4-4
4.5 Spectral Analysis and Retrievals.....	4-5
4.6 Tropospheric CH ₄ Volume Mixing Ratios	4-8
4.7 Conclusions.....	4-11
4.8 Acknowledgments	4-12
4.9 Appendix: Pressure Broadening of the CH ₄ 2ν ₃ Band	4-12
4.10 Appendix: Correlation of HF and CH ₄ in the Lower and Mid Stratosphere: the Determination of b(t).....	4-13

4.11 References.....	4-16
Appendix Technical Documentation for the Caltech Column Observatory.....	5-1
A.1 Summary.....	5-1
A.2 Instrumentation.....	5-2
A.2.1 Bruker IFS125 Spectrometer.....	5-2
A.2.1.1 Laser (Spectra-Physics 117A).....	5-2
A.2.1.2 Scanner.....	5-3
A.2.1.3 Detectors.....	5-3
A.2.1.4 Tungsten Lamp.....	5-4
A.2.1.5 Valves and Vacuum System.....	5-5
A.2.1.6 Small Devices with Control Area Network Boards.....	5-6
A.2.1.7 Electronics Systems.....	5-6
A.2.1.8 HTML Software Interface.....	5-8
A.2.1.9 IFS125 Direct Commands and Allowed Values.....	5-9
A.2.1.10 Alignment Procedure.....	5-12
A.2.1.11 Previous Alignment Results.....	5-16
A.2.1.12 Acceptance Test Standards.....	5-17
A.2.1.13 HCl Cells.....	5-19
A.2.2 Bruker Solar Tracker.....	5-20
A.2.2.1 Solar Tracker Direct RS232 Commands.....	5-20
A.2.2.2 Solar Tracker Installation.....	5-21
A.2.3 Telescope Dome.....	5-23
A.2.3.1 Dome Direct RS232 Commands:.....	5-24
A.2.4 Weather Station.....	5-25
A.2.4.1 Direct RS232 Commands:.....	5-25
A.2.4.2 Barometric Pressure (S1080Z).....	5-25
A.2.4.3 Relative Humidity and Air Temperature (S1276Z).....	5-26
A.2.4.4 Wind Speed and Direction (S1146Z).....	5-26
A.2.4.5 Pyranometer (S1114Z).....	5-26
A.2.4.6 Precipitation Detector (S1391Z).....	5-26
A.2.4.7 Leaf Wetness Sensor (S1169).....	5-26

A.2.4.8 Mercury Manometer	5-26
A.2.5 Other Laboratory Instrumentation	5-28
A.2.5.1 NTP-GPS Receiver	5-28
A.2.5.2 Network Camera	5-28
A.2.5.3 Scroll Pump	5-28
A.2.5.4 Scroll Pump Pressure Sensor	5-29
A.2.6 Network and Communication	5-30
A.2.6.1 Network Information	5-30
A.2.6.2 Modem.....	5-30
A.2.7 Power Systems	5-31
A.2.7.1 Uninterruptible Power Supply	5-31
A.2.8 Digital and Analog Signals	5-32
A.2.8.1 Control Using Digital Lines.....	5-32
A.2.8.2 Monitoring of Analog Inputs	5-32
A.2.8.3 Reference and Background Information	5-33
A.2.9 Laboratory structure	5-35
A.2.9.1 Container	5-35
A.2.9.2 Heater – Air Conditioner Unit	5-35
A.3 Data Acquisition Software	5-36
A.3.1 Data Acquisition Software Overview	5-36
A.3.2 Data Acquisition Source Code Files.....	5-37
A.3.3 Organization of Data	5-40
A.3.4 Telemetry Data	5-42
A.3.5 Quick Command Tree for ifsdoit.....	5-45
A.3.6 Detailed Description of ifsdoit Commands	5-47
A.3.7 Routine Monitoring of the Data Acquisition.....	5-51
A.3.8 Queuing Directories to Repeat the Overnight Analysis.....	5-52
A.3.9 Hercules Computer Shutdown Instructions.....	5-52
A.3.10 Useful QNX Commands	5-53
A.3.11 CVS Software Archive.....	5-54
A.4 Data Transfer, Archive, and Processing	5-56

A.4.1 Removable Disks.....	5-56
A.4.2 RAID at Caltech	5-58
A.4.3 MD5SUM Tool: dircksum.....	5-60
A.4.4 Slice-IPP Fourier Transform Software	5-61
A.4.4.1 Fourier-Transform Using Slice-IPP.....	5-61
A.4.4.2 Bruker Acronyms Contained in the IFS125 Spectral Headers	5-61
A.4.4.3 Additional Acronyms Defined for the IFS125 Spectral Headers	5-63
A.4.4.4 Filenaming Convention.....	5-64
A.5 General Logistics	5-65
A.5.1 Contact Information and Account Numbers.....	5-65
A.5.2 Caltech FTS Site.....	5-66
A.5.2.1 Caltech Contact Information and Logistics.....	5-66
A.5.2.2 Caltech Network Connectivity	5-66
A.5.3 Park Falls FTS Site.....	5-67
A.5.3.1 Park Falls Contact Information and Logistics.....	5-67
A.5.3.2 Park Falls Network Connectivity	5-68
A.5.4 Darwin FTS Site.....	5-70
A.5.4.1 Darwin Contact Information and Logistics	5-70
A.5.4.2 Darwin Network Connectivity.....	5-71

List of Figures

Figure 2.1 Photograph and Block Diagram of the Automated FTS Observatory.	2-4
Figure 2.2 Signal-to-Noise Ratio and Near-IR Absorptions in FTS Solar Spectrum.....	2-6
Figure 2.3 Correlation Between Retrieved Column O ₂ and Dry Surface Pressure.	2-14
Figure 2.4 Spectral Retrievals During One Clear and One Partly Cloudy Day.....	2-16
Figure 2.5 Aircraft Profile Measurement of In Situ CO ₂	2-21
Figure 2.6 Comparison of Column and Integrated Aircraft CO ₂ Profiles	2-22
Figure 2.7 Diurnal and Seasonal Column CO ₂ Measurements.	2-25
Figure 3.1 WISCLAND Landcover Classification.....	3-5
Figure 3.2 Column, In Situ, and Eddy Covariance Measurements of CO ₂	3-7
Figure 3.3 TransCom Model Predictions of Seasonal Cycle..	3-9
Figure 3.4 Demonstration of Column and Eddy Covariance Observations of NEE.	3-15
Figure 3.5 Column CO ₂ Change Attributed to NEE and Transport.....	3-16
Figure 3.6 Drawdown Observed During a Four-Hour Period.....	3-18
Figure 4.1 Spectral Fits of CH ₄ and HF for a Kitt Peak Solar Absorption Spectrum.	4-7
Figure 4.2 Time Series of Column-Average CH ₄ and Column HF.	4-8
Figure 4.3 CH ₄ –HF Slope Values from the HALOE, MkIV, and Kitt Peak Data.	4-9
Figure 4.4 Time Series of Kitt Peak Tropospheric CH ₄ VMR.....	4-10
Figure 4.5 Determination of CH ₄ –HF Slope Values.	4-14
Figure 4.6 CH ₄ and HF Averaging Kernels for a Kitt Peak Spectrum	4-15

List of Tables

Table 2.1. Mean and standard deviation of column CO ₂ measurements during a one-hour observational period around local noon.....	2-16
---	------

List of Abbreviations

CASA – Carnegie-Ames-Stanford Approach biogeochemical model

COBRA – CO₂ Boundary-layer Regional Airborne experiment

FTS – Fourier transform spectrometry or Fourier transform spectrometer

GAGE/AGAGE – Global Atmospheric Gases Experiment / Advanced Global Atmospheric Gases Experiment

GFIT – Spectral retrieval analysis software

GOSAT – Greenhouse Gases Observing Satellite

HALOE – Halogen Occultation Experiment

HITRAN – High-Resolution Transmission molecular absorption database

INTEX-NA – Intercontinental Chemical Transport Experiment – North America

MATCH – Multiscale Atmospheric Transport and Chemistry model

MOPPIT – Measurements of Pollution in the Troposphere

NDSC – Network for the Detection of Stratospheric Change

NEE – Net Ecosystem Exchange

OCO – Orbiting Carbon Observatory

SCIAMACHY – Scanning Imaging Absorption Spectrometer for Atmospheric Chartography

SZA – Solar Zenith Angle

TCCON – Total Carbon Column Observing Network

TransCom – Atmospheric Tracer Transport Model Intercomparison Project

UARS – Upper Atmosphere Research Satellite

WISCLAND – Wisconsin Initiative for Statewide Cooperation on Landscape Analysis and
Data

Chapter 1

INTRODUCTION

1.1 The Global Carbon Budget

An increasing body of observations gives a collective picture of a warming world and other changes in the climate system [(IPCC), 2001]. The atmospheric constituents with current importance to climate are H₂O, CO₂, O₃, CH₄, N₂O, CFC-11, and CFC-12 [Ramanathan *et al.*, 1987]. Close correlations between CO₂, CH₄, and temperature are observed in the Vostok ice core record during the past 420,000 years [Petit *et al.*, 1999; Fischer *et al.*, 1999], suggesting that past climate change is in part forced by changes in atmospheric concentrations of greenhouse gases. Although the atmospheric concentration of CH₄ and the magnitude of CH₄ fluxes are much lower than that of CO₂ [Fung *et al.*, 1991; Houweling *et al.*, 1999], CH₄ plays an important role in the Earth's radiative balance. The instantaneous forcing of each additional CH₄ molecule in the atmosphere is 43 times greater than that for a molecule of CO₂ [Lashof and Ahuja, 1990]. Better understanding of both CO₂ and CH₄ is critical to predicting the Earth's radiative budget.

The global budgets of CO₂ and CH₄ have been altered by anthropogenic activity. Atmospheric CO₂ concentrations have increased from 280 ppmv in pre-industrial times to ~370 ppmv in 1999, and are currently increasing at a rate of 1 – 2 ppmv yr⁻¹ [(IPCC), 2001]. This increase is mainly anthropogenic, and is attributed to fossil fuel consumption [Marland, 2000] and land use change [Houghton, 1999]. The net global release of CO₂ caused by the burning of fossil fuels is one of the best-known values in the global carbon cycle [Marland, 2000]. The discrepancy between CO₂ release by burning of fossil fuels and CO₂ accumulation in the atmosphere is attributed to uptake by oceans and the terrestrial biosphere [Battle *et al.*, 2000; Keeling *et al.*, 1993; Keeling and Shertz, 1992]. CH₄ concentrations have also increased rapidly, from ~0.685 ppmv to ~1.745 ppmv between 1750 and 1998 [Dlugokencky *et al.*, 1998]. During the past two decades, the growth rate of CH₄ has varied between 0 and 0.015 ppmv yr⁻¹ [Dlugokencky *et al.*, 1998],

but the cause of this variability is poorly understood. The decline in growth rate may be due to decreased northern wetland emission rates [*Hogan and Harriss, 1994*] or increases in tropospheric OH [*Bekki et al., 1994*]. Isotopic records of atmospheric CH₄ suggest an anomaly in sources or sinks involving more than one causal factor [*Lowe et al., 1997; Mak et al., 2000*]. The variable increase of atmospheric CH₄ is likely due to a small imbalance between poorly-characterized sources and sinks.

It is clear that a significant source of uncertainty in the prediction of climate change is the future concentrations of the greenhouse gases themselves [*Rayner et al., 1996*]. Uncertainty in future trends for these gases arises from uncertainty in their current budget. After 30 years of measurements in the atmosphere and oceans, many unknowns still remain in the global CO₂ budget. The magnitude of sources and sinks of CO₂ and other greenhouse gases are currently inferred from in situ measurements at two global networks of surface sites, operated by the National Oceanic and Atmospheric Administration (NOAA) and the Scripps Institute of Oceanography [*GLOBALVIEW-CO2, 2005; Conway et al., 1994; Keeling et al., 1995*]. Studies have combined in situ measurements of CO₂ with global scale transport models to estimate regional-scale surface exchange of CO₂ using inversion techniques [*Gurney et al., 2002; Rayner et al., 1999; Tans et al., 1990*]. This has proven difficult, in part due to limitations in the surface measurements. Although the measurements are highly accurate, they have limited spatial coverage, are confined to the planetary boundary layer, and are biased to specific weather conditions. Because exchange and transport are correlated on diurnal and seasonal timescales, errors in transport fields may be aliased into the inferred exchange terms as “rectifier” effects [*Denning et al., 1996a; Gurney et al., 2002*].

The atmospheric column integral of CO₂ and CH₄ may be effective in constraining the global carbon budget [*Olsen and Randerson, 2004*]. Column measurements sample a larger portion of the atmosphere than surface in situ measurements. Because the column is insensitive to vertical mixing, the column integral should be largely unaffected by diurnal fluctuations in the boundary layer and should exhibit much less variability than surface data, thus avoiding rectifier effects while retaining information about surface fluxes [*Gloor et al., 2000*]. Model predictions show that a few column measurements at carefully

selected sites could constrain the global carbon budget [*Gloor et al.*, 2000; *Rayner and O'Brien*, 2001].

1.2 Remote Sensing Techniques

Remote sensing methods can be used to obtain the column integrals of CO₂, CH₄, and other atmospheric species. Because molecules possess quantized internal energy levels, they absorb and emit electromagnetic radiation at discrete frequencies. The electromagnetic spectrum of the atmosphere contains features that are characteristic of its constituents, and can be used for their identification and quantification. The features that we observe in the atmosphere are due to electronic, vibrational, and rotational transitions of molecules and atoms. Electronic transitions are typically observed in the visible and ultraviolet spectral regions. Vibrational transitions are observed in the near-infrared and mid-infrared spectral regions. Rotational transitions within a vibrational state are observed in the far-infrared and microwave spectral regions. Atmospheric remote sensing is possible from the ground, from aircraft, from balloons, and from space, with observation of radiation either from an external source (absorption spectroscopy) or from the atmospheric blackbody signal (emission spectroscopy).

Solar absorption spectroscopy has been used to measure the Earth's atmosphere for over a century. The solar absorption spectrum was first measured by Joseph von Fraunhofer using a grating instrument. In 1879, Marie Alfred Cornu predicted that the short wavelength limit of the observed solar radiation must be caused by an absorber in the Earth's atmosphere [*Cornu*, 1879b; *Cornu*, 1879a; *Cornu*, 1890]. This correct deduction of the strong UV O₃ absorptions was followed by identifications from Sir Walther Noel Hartley, J. Chappuis, and Sir William Huggins [*Hartley*, 1881; *Huggins*, 1889]. By the 20th century, ground-based remote infrared sensing used prisms and grating spectrometers to measure the sun's light. High-altitude observatories minimized spectral interference, and measurements at sunset and sunrise maximized the atmospheric path for improved detection of trace species. The first systematic study of solar irradiance at the Earth's surface was conducted by Samuel Pierpont Langley, using these methods at the summit of Mt. Whitney, California [*Langley*, 1900]. A stable spectrometer, using a double monochromator with quartz prisms, was developed by Gordon M. B. Dobson to quantify

the vertical column density of O₃ [Dobson, 1968]. The Dobson spectrometer is the direct predecessor of modern-day atmospheric remote sensing.

Fourier Transform Spectrometry (FTS) is the direct descendant of these early spectroscopic measurements. The FTS is an adapted Michelson interferometer [Michelson, 1891; Michelson, 1892] with a movable mirror. After a collimated beam is split by the beamsplitter, the two resulting beams travel different paths and are then reflected back onto the beamsplitter, where they recombine. After being recorded by a detector as a function of optical path difference, the interference pattern can be Fourier transformed to determine the spectrum in frequency space. The instrument provides simultaneous measurement of all spectral points, with an operational spectral range that is determined by the material of the beamsplitter and detectors. The FTS is the most accurate general-purpose passive spectrometer available, with high optical efficiency and throughput, simultaneous observations at all wavelengths and a wide spectral range [Brault, 1996]. In addition, instrument distortions are often calculable and correctable. Recent advances in FTS offer several additional advantages. Computation and storage space are now sufficient to allow interferograms to be acquired continuously without the necessity of co-adding, and interferogram resampling methods exploit 24-bit delta-sigma analog-digital converters to improve instrumental signal-to-noise [Brault, 1996].

Recent work has shown that column-average CO₂ and CH₄ volume mixing ratios (VMR) can be retrieved with high precision from ground-based near-infrared solar absorption spectra [Yang *et al.*, 2002; Warneke *et al.*, 2005; Dufour *et al.*, 2004]. The near-infrared spectral region has been chosen due both to spectroscopic and instrumental considerations. Spectroscopically, the near-infrared spectral region contains optically thin CO₂ and CH₄ transitions, with O₂ lines that can be used to calculate column-average CO₂ and CH₄ with improved precision. The near-infrared is near the peak of the solar Planck function, maximizing signal-to-noise. Thermal emission from the atmosphere and instrument are negligible compared with direct sunlight, simplifying calibration and radiative transfer calculations. The major instrumental advantage is that sensitive, room-temperature detectors are now available in the near-infrared spectral region. This eliminates the need for liquid N₂ and facilitates autonomous data collection. For these reasons, the near-

infrared spectral region is also the choice for current and future space-based observations, such as the Scanning Imaging Absorption Spectrometer for Atmospheric Chartography (SCIAMACHY), the Orbiting Carbon Observatory (OCO), and the Greenhouse Gases Observing Satellite (GOSAT).

1.3 Outline of the Dissertation

This work extends FTS remote sensing to better constrain the global carbon budget through measurements of column-average CO₂ and CH₄ concentrations.

Chapter 2 describes an automated observatory for measuring atmospheric column abundances of CO₂, CH₄, CO, N₂O, H₂O, HDO, O₂, and HF using near-infrared spectra of the sun obtained with a high spectral resolution FTS. This is the first dedicated observatory in a network of ground-based FTS sites, named the Total Carbon Column Observing Network (TCCON). The observatory is located in the Chequamegon National Forest at the WLEF Tall Tower site, 12 kilometers east of Park Falls, Wisconsin. Under clear sky conditions, ~0.1% measurement precision is demonstrated for the retrieved column CO₂ abundances. During the Intercontinental Chemical Transport Experiment – North America and CO₂ Boundary-layer Regional Airborne Experiment campaigns in Summer 2004, the DC-8 and King Air aircraft recorded eight in situ CO₂ profiles over the WLEF site. Comparison of the integrated aircraft profiles and CO₂ column abundances shows a small bias (~2%), but an excellent correlation.

Chapter 3 demonstrates the potential of column measurements to constrain CO₂ exchange on seasonal and diurnal timescales. To evaluate carbon exchange on seasonal timescales, CO₂ measurements from May 2004 – March 2006 are compared to in situ measurements and TransCom model predictions. The results are consistent with theoretical predictions that column measurements in the Northern Hemisphere will generally be representative of Northern Hemispheric CO₂ exchange over seasonal timescales. In addition, the results suggest that the Carnegie-Ames-Stanford Approach (CASA) model underpredicts the seasonal amplitude observed in the column. To examine carbon exchange on daily timescales, the column measurements are compared to eddy covariance measurements acquired in and above the convective boundary layer. The results show that the column

measurements are sufficiently precise to observe CO₂ exchange. However, the results are limited by the difficulty in constraining concentration changes due to transport.

Chapter 4 presents a technique to retrieve column-average CH₄ VMRs using spectra from the Kitt Peak National Solar Observatory. Simultaneous measurements of CH₄, O₂, and HF are used together with known information about the stratospheric relationship of CH₄ and HF to calculate tropospheric column-average CH₄ VMRs. Using this technique, tropospheric column-average CH₄ VMRs are determined with a precision of ~0.5%. These display behavior similar to Mauna Loa in situ surface measurements, with a seasonal peak-to-peak amplitude of approximately 30 ppbv and a nearly linear increase between 1977 and 1983 of 18.0 ± 0.8 ppbv yr⁻¹, slowing significantly after 1990.

The appendix provides detailed technical information regarding the instrumentation and operation of the three automated Caltech FTS observatories. This documentation is intended as a resource for future users.

1.4 References

- Intergovernmental Panel on Climate Change (2001), *Climate Change 2001: The Scientific Basis*, Cambridge University Press, Cambridge.
- Battle, M., M. L. Bender, P. P. Tans, J. W. C. White, J. T. Ellis, T. Conway, and R. J. Francey (2000), Global carbon sinks and their variability inferred from atmospheric O₂ and δ¹³C, *Science*, 287, 2467-2470.
- Bekki, S., K. S. Law, and J. A. Pyle (1994), Effect of ozone depletion on atmospheric CH₄ and CO concentrations, *Nature*, 371, 595-597.
- Brault, J. W. (1996), New approach to high-precision Fourier transform spectrometer design, *Appl. Opt.*, 35, 2891-2896.
- Conway, T. J., P. P. Tans, L. S. Waterman, and K. W. Thoning (1994), Evidence for interannual variability of the carbon cycle from the National Oceanic and Atmospheric Administration Climate Monitoring and Diagnostics Laboratory Global Air Sampling Network, *J. Geophys. Res.*, 99, 22831-22855.
- Cornu, A. (1879a), Sur l'absorption par l'atmosphère des radiations ultra-violettes, C. R. l'Académie. Sci., *Ser. II Univers*, 88, 1285-1290.

- Cornu, A. (1879b), Sur la limite ultra-violette du spectre solaire, C. R. l'Academie. Sci., *Ser. II Univers*, 88, 1101-1108.
- Cornu, A. (1890), Sur la limite ultra-violette du spectre solaire, d'apres des cliches obtenus par M. le Dr. O. Simony au sommet du pic de Teneriffe, C. R. l'Academie. Sci., *Ser. II Univers*, 111, 941-947.
- Denning, A. S., G. J. Collatz, C. G. Zhang, D. A. Randall, J. A. Berry, P. J. Sellers, G. D. Colello, and D. A. Dazlich (1996), Simulations of terrestrial carbon metabolism and atmospheric CO₂ in a general circulation model: 1. Surface carbon fluxes, *Tellus*, 48, 521-542.
- Dlugokencky, E. J., K. A. Masarie, P. M. Lang, and P. P. Tans (1998), Continuing decline in the growth rate of the atmospheric methane burden, *Nature*, 393, 447-450.
- Dobson, G. M. B. (1968), Forty years' research on atmospheric ozone at Oxford: A history, *Appl. Opt.*, 7, 387-405.
- Dufour, E., F. M. Breon, and P. Peylin (2004), CO₂ column averaged mixing ratio from inversion of ground-based solar spectra, *J. Geophys. Res.*, 109, doi:10.1029/2003JD004469.
- Fischer, H., M. Wahlen, J. Smith, D. Mastroianni, and B. Deck (1999), Ice core records of atmospheric CO₂ around the last three glacial terminations, *Science*, 283, 1712-1714.
- Fung, I., J. John, J. Lerner, E. Matthews, M. Prather, L. P. Steele, and P. J. Fraser (1991), 3-Dimensional model synthesis of the global methane cycle, *J. Geophys. Res.*, 96, 13033-13065.
- GLOBALVIEW-CO2 (2005), GLOBALVIEW-CO2: Cooperative Atmospheric Data Integration Project - Carbon Dioxide. CD-ROM, National Oceanic and Atmospheric Administration Climate Monitoring and Diagnostics Laboratory, Boulder, Colorado., edited.
- Gloor, M., S. M. Fan, S. Pacala, and J. Sarmiento (2000), Optimal sampling of the atmosphere for purpose of inverse modeling: A model study, *Glob. Biogeochem. Cy.*, 14, 407-428.
- Gurney, K. R., R. M. Law, A. S. Denning, P. J. Rayner, D. Baker, P. Bousquet, L. Bruhwiler, Y. H. Chen, P. Ciais, S. Fan, I. Y. Fung, M. Gloor, M. Heimann, K. Higuchi, J. John, T. Maki, S. Maksyutov, K. Masarie, P. Peylin, M. Prather, B. C. Pak,

- J. Randerson, J. Sarmiento, S. Taguchi, T. Takahashi, and C. W. Yuen (2002), Towards robust regional estimates of CO₂ sources and sinks using atmospheric transport models, *Nature*, *415*, 626-630.
- Hartley, W. N. (1881), On the absorption of solar rays by atmospheric ozone, *J. Chem. Soc.*, *39*, 111-128.
- Hogan, K. B., and R. C. Harriss (1994), A dramatic decrease in the growth rate of atmospheric methane in the Northern Hemisphere during 1992 - Comment, *Geophys. Res. Lett.*, *21*, 2445-2446.
- Houghton, R. A. (1999), The annual net flux of carbon to the atmosphere from changes in land use 1850-1990, *Tellus*, *51*, 298-313.
- Houweling, S., T. Kaminski, F. Dentener, J. Lelieveld, and M. Heimann (1999), Inverse modeling of methane sources and sinks using the adjoint of a global transport model, *J. Geophys. Res.*, *104*, 26137-26160.
- Huggins, W. (1889), On the limit of solar and stellar light in the ultra-violet part of the spectrum, *Proc. R. Soc. London, A*, *46*, 133-135.
- Keeling, C. D., T. P. Whorf, M. Wahlen, and J. Vanderpligt (1995), Interannual extremes in the rate of rise of atmospheric carbon dioxide since 1980, *Nature*, *375*, 666-670.
- Keeling, R. F., R. P. Najjar, M. L. Bender, and P. P. Tans (1993), What atmospheric oxygen measurements can tell us about the global carbon cycle, *Glob. Biogeochem. Cy.*, *7*, 37-67.
- Keeling, R. F., and S. R. Shertz (1992), Seasonal and interannual variations in atmospheric oxygen and implications for the global carbon cycle, *Nature*, *358*, 723-727.
- Langley, S. P. (1900), The absorption lines in the infrared spectrum of the sun, *Annals of the Astrophysical Observatory of the Smithsonian Institution*, *1*, 69-75.
- Lashof, D. A., and D. R. Ahuja (1990), Relative contributions of greenhouse gas emissions to global warming, *Nature*, *344*, 529-531.
- Lowe, D. C., M. R. Manning, G. W. Brailsford, and A. M. Bromley (1997), The 1991-1992 atmospheric methane anomaly: Southern Hemisphere ¹³C decrease and growth rate fluctuations, *Geophys. Res. Lett.*, *24*, 857-860.

- Mak, J. E., M. R. Manning, and D. C. Lowe (2000), Aircraft observations of $\delta^{13}\text{C}$ of atmospheric methane over the Pacific in August 1991 and 1993: Evidence of an enrichment in $^{13}\text{CH}_4$ in the Southern Hemisphere, *J. Geophys. Res.*, *105*, 1329-1335.
- Marland, G., T.A. Boden, and R.J. Andres (2000), Global, Regional, and National CO_2 Emissions, in Trends: A Compendium of Data on Global Change, edited, Carbon Dioxide Information Analysis Center, Oak Ridge National Laboratory, Oak Ridge.
- Michelson, A. A. (1891), Visibility of interference-fringes in the focus of a telescope, *Philos. Mag. B*, *31*, 256-259.
- Michelson, A. A. (1892), On the application of interference-methods to spectroscopic measurements, *Philos. Mag. B*, *34*, 280.
- Olsen, S. C., and J. T. Randerson (2004), Differences between surface and column atmospheric CO_2 and implications for carbon cycle research, *J. Geophys. Res.*, *109*, doi:10.1029/2003JD003968.
- Petit, J. R., J. Jouzel, D. Raynaud, N. I. Barkov, J. M. Barnola, I. Basile, M. Bender, J. Chappellaz, M. Davis, G. Delaygue, M. Delmotte, V. M. Kotlyakov, M. Legrand, V. Y. Lipenkov, C. Lorius, L. Pepin, C. Ritz, E. Saltzman, and M. Stievenard (1999), Climate and atmospheric history of the past 420,000 years from the Vostok ice core, Antarctica, *Nature*, *399*, 429-436.
- Ramanathan, V., L. Callis, R. Cess, J. Hansen, I. Saksen, W. Kuhn, A. Lacis, F. Luther, J. Mahlman, R. Reck, and M. Schlesinger (1987), Climate-chemical interactions and effects of changing atmospheric trace gases, *Rev. Geophys.*, *25*, 1441-1482.
- Rayner, P. J., I. G. Enting, R. J. Francey, and R. Langenfelds (1999), Reconstructing the recent carbon cycle from atmospheric CO_2 , $\delta^{13}\text{C}$ and O_2/N_2 observations, *Tellus*, *51*, 213-232.
- Rayner, P. J., I. G. Enting, and C. M. Trudinger (1996), Optimizing the CO_2 observing network for constraining sources and sinks, *Tellus*, *48*, 433-444.
- Rayner, P. J., and D. M. O'Brien (2001), The utility of remotely sensed CO_2 concentration data in surface source inversions, *Geophys. Res. Lett.*, *28*, 175-178.
- Tans, P. P., I. Y. Fung, and T. Takahashi (1990), Observational constraints on the global atmospheric CO_2 budget, *Science*, *247*, 1431-1438.

Warneke, T., Z. Yang, S. Olsen, S. Korner, J. Notholt, G. C. Toon, V. Velazco, A. Schulz, and O. Schrems (2005), Seasonal and latitudinal variations of column averaged volume-mixing ratios of atmospheric CO₂, *Geophys. Res. Lett.*, 32, doi:10.1029/2004GL021597.

Yang, Z. H., G. C. Toon, J. S. Margolis, and P. O. Wennberg (2002), Atmospheric CO₂ retrieved from ground-based near IR solar spectra, *Geophys. Res. Lett.*, 29, doi:10.1029/2001GL014537.

Chapter 2

CARBON DIOXIDE COLUMN ABUNDANCES AT THE WISCONSIN TALL TOWER SITE*

*Adapted from R.A. Washenfelder, G.C. Toon, J.-F. Blavier, Z. Yang, N.T. Allen, P.O. Wennberg, S.A. Vay, D.M. Matross, and B.C. Daube (2006), *Journal of Geophysical Research, in press*.

2.1 Abstract

We have developed an automated observatory for measuring atmospheric column abundances of CO₂ and O₂ using near-infrared spectra of the sun obtained with a high spectral resolution Fourier Transform Spectrometer (FTS). This is the first dedicated laboratory in a new network of ground-based observatories named the Total Carbon Column Observing Network. This network will be used for carbon cycle studies and validation of spaceborne column measurements of greenhouse gases. The observatory was assembled in Pasadena, California, and then permanently deployed to northern Wisconsin during May 2004. It is located in the heavily forested Chequamegon National Forest at the WLEF Tall Tower site, 12 km east of Park Falls, Wisconsin. Under clear sky conditions, ~0.1% measurement precision is demonstrated for the retrieved column CO₂ abundances. During the Intercontinental Chemical Transport Experiment – North America and CO₂ Boundary-layer Regional Airborne Experiment campaigns in summer 2004, the DC-8 and King Air aircraft recorded eight in situ CO₂ profiles over the WLEF site. Comparison of the integrated aircraft profiles and CO₂ column abundances shows a small bias (~2%) but an excellent correlation.

2.2 Introduction

In the last two decades, numerous studies [e.g. Gurney *et al.*, 2002; Rayner *et al.*, 1999; Tans *et al.*, 1990] have combined in situ measurements of CO₂ obtained from a global network of surface sites [*GLOBALVIEW-CO2*, 2005] with global transport models to

estimate regional-scale surface exchange of CO₂. Although the surface measurements are highly accurate, their limited spatial coverage and proximity to local sources and sinks make these estimates quite sensitive to the errors in the transport model (e.g. vertical mixing), particularly for sites located in the continental interior. In particular, because the surface fluxes and vertical transport are correlated on diurnal and seasonal timescales, errors in transport fields are aliased into the inferred exchange term as so-called "rectifier" effects [Denning *et al.*, 1996a; Gurney *et al.*, 2002].

Precise and accurate CO₂ column measurements can complement the existing in situ network and provide information about CO₂ exchange on larger geographic scales. Unlike the near-surface volume mixing ratio (VMR), the column integral of the CO₂ profile is not altered by diurnal variations in the height of the boundary layer. As a result, it exhibits less spatial and temporal variability than near-surface in situ data, while retaining information about surface fluxes [Gloor *et al.*, 2000]. Because few CO₂ column measurements are available, understanding of their potential information content has been largely limited to simulations [Rayner and O'Brien, 2001; Olsen and Randerson, 2004]. These studies show that CO₂ column measurements at carefully selected sites could be effective in constraining global-scale carbon budgets [Rayner and O'Brien, 2001].

Three recent analyses of near-infrared FTS solar spectra obtained by Fourier Transform Spectrometers (FTS) demonstrate that column-averaged CO₂ VMRs can be retrieved with high precision [Yang *et al.*, 2002; Dufour *et al.*, 2004; Warneke *et al.*, 2005]. The near-infrared spectral region is an appropriate observational choice for several reasons: (i) it is near the peak of the solar Planck function, expressed in units of photons/s/m²/sr/cm⁻¹, maximizing signal-to-noise; (ii) retrievals from O₂ absorption lines in the near-infrared spectral region provide an internal standard; (iii) highly sensitive uncooled detectors are available for this region. For these reasons, the near-infrared region has also been chosen by several space-based column observatories, including the Orbiting Carbon Observatory (OCO), the Scanning Imaging Absorption Spectrometer for Atmospheric Chartography (SCIAMACHY), and the Greenhouse Gases Observing Satellite (GOSAT).

Most of the existing FTS instruments from the Network for the Detection of Stratospheric Change (NDSC) [*Kurylo and Solomon, 1990*] are not well suited for measurement of CO₂ and other greenhouse gases. Most NDSC sites are located at high altitude to facilitate stratospheric measurements. To understand the sources and sinks of greenhouse gases, however, observatories should be located at low altitude. In addition, the existing NDSC sites are optimized for observations of the mid-infrared spectral region, with KBr beamsplitters, aluminum optics, and mid-infrared detectors. Although many trace atmospheric constituents have fundamental vibrational-rotational absorptions in the mid-infrared spectral region, the near-infrared spectral region is a better choice for measuring CO₂ and other greenhouse gases.

The Total Carbon Column Observing Network is a new network of ground-based FTS sites. We describe the first dedicated laboratory in this network. This is an automated FTS observatory developed for highly precise, ground-based solar absorption spectrometry in the near-infrared spectral region. Atmospheric column abundances of CO₂, CH₄, CO, N₂O, H₂O, HDO, O₂, and HF can be retrieved from the observed near-infrared spectral region. The observatory was assembled in Pasadena, California and then deployed to Park Falls, Wisconsin during May 2004. We compare the column CO₂ results with integrated in situ aircraft profiles, and present the CO₂ column values for May 2004 – October 2005. Readers interested in these results may wish to skip the detailed instrumental description in Section 2.2 and proceed directly to Section 2.3.

2.3 Instrumentation

2.3.1 Bruker 125HR Spectrometer

Solar spectra are acquired at high spectral resolution using a Bruker 125HR FTS housed in a custom laboratory (Figure 2.1). The Bruker 125HR has been substantially improved over its predecessor, the Bruker 120HR. One important improvement is the implementation of the interferogram sampling method described by *Brault* [1996], that takes advantage of modern 24-bit delta-sigma analog-digital converters to improve the signal-to-noise ratio.

The spectrometer described here has been optimized for measurements in the near-infrared spectral region, with gold-coated optics and a CaF_2 beamsplitter with broad-band coating. Interferograms are simultaneously recorded by two uncooled detectors. Complete spectral coverage from $3,800 - 15,500 \text{ cm}^{-1}$ is obtained by simultaneous use of an InGaAs detector ($3,800 - 12,000 \text{ cm}^{-1}$) and Si-diode detector ($9,500 - 30,000 \text{ cm}^{-1}$) in dual-acquisition mode, with a dichroic optic (Omega Optical, $10,000 \text{ cm}^{-1}$ cut-on). A filter (Oriel Instruments 59523; $15,500 \text{ cm}^{-1}$ cut-off) prior to the Si diode detector blocks visible light, which would otherwise be aliased into near-infrared spectral domain. The observed

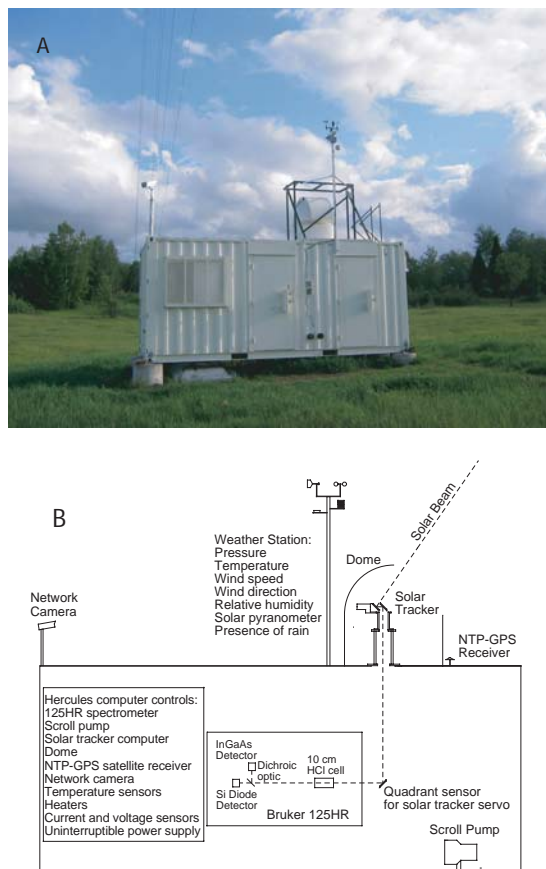


Figure 2.1. (a) Photograph of the automated FTS laboratory, located 25 m south of the WLEF Tall Tower. A telescope dome, weather station, and network camera are mounted on the roof. (b) Block diagram showing the laboratory. A servo-controlled solar tracker directs the solar beam through a CaF_2 window to the Bruker 125HR spectrometer in the laboratory. A 10 cm cell with 5.1 hPa HCl is mounted in the source compartment of the 125HR, prior to the input field stop. Two detectors simultaneously record the solar spectrum in the $3,900 - 15,500 \text{ cm}^{-1}$ region. The Hercules computer uses custom data acquisition software to monitor and control the 125HR spectrometer, solar tracker, telescope dome, weather station, camera, scroll pump, GPS satellite time server, temperature sensors, and heaters.

spectral region includes absorption bands of CO₂, CH₄, CO, N₂O, H₂O, HDO, O₂, and HF. Spectra from the Si-diode detector are not analyzed in this work, but are useful for comparison with OCO and other future satellite instruments measuring the $b^1\Sigma_g^+(v=0) \leftarrow X^3\Sigma_g^-(v=0)$ O₂ transition (A-band) between 12,950 and 13,170 cm⁻¹. For the spectra obtained here, we use a 45 cm optical path difference and a 2.4 mrad field of view, yielding an instrument line shape that has a full-width at half-maximum of 0.014 cm⁻¹. This is sufficient to fully resolve individual absorption lines in the near-infrared. The input optics uses an off-axis parabolic mirror that is the same type as the collimating mirror. Hence the external field of view is also 2.4 mrad, and the instrument accepts only a small fraction of the 9.4 mrad solar disk. The beam diameter is stopped down to 3.5 cm to reduce the saturation of the detectors and signal amplifiers. Figure 2.2a shows a typical spectrum, acquired in 110 s, with signal-to-noise ratios of ~900:1 and ~500:1 for the InGaAs and Si diode detectors, respectively. The observed intensity is the product of the solar Planck function with the instrument response.

To maintain stability of the optical alignment, the internal temperature of the spectrometer is controlled between 28 – 30° C. To reduce acoustic noise and eliminate refractive inhomogeneities, the internal pressure is maintained at less than 2 hPa using a Varian TriScroll 300 scroll pump. The spectrometer is evacuated once per day, before sunrise, and has a leak rate less than 2 hPa day⁻¹. The instrument lineshape is monitored using narrow HCl lines in the first overtone band ($\nu_0 = 5882$ cm⁻¹). A 10 cm cell with 30' wedged Infrasil windows containing 5.1 hPa of HCl gas is permanently mounted in the source compartment, prior to the entrance field stop wheel, as shown in Figure 2.1b. Due to space constraints, the sample compartment typically supplied with the 125HR is not used.

2.3.2 Laboratory and Other Instrumentation

The 125HR spectrometer is mounted inside a modified 6.1 × 2.4 × 2.6 m steel shipping container. The container is equipped with an air conditioning and heating wall unit, power (110 VAC and 208 VAC), lights, and telephone connection. The interior of the container is insulated with 9.0 cm of R19 fiberglass covered with 0.32 cm thick aluminum sheet. These materials were chosen to minimize outgassing that may otherwise interfere with spectral observations.

The optical assembly (solar tracker) that transfers the direct solar beam from the roof of the container to the FTS was purchased from Bruker Optics. It consists of a servo-controlled assembly with two gold-coated mirrors that rotate in azimuth ($0^\circ - 310^\circ$) and elevation ($-5^\circ - +90^\circ$). The solar tracker has two operational modes: pointing to the calculated solar position and active servo-controlled tracking. Initially, the solar tracker is pointed toward the calculated solar ephemeris. This position is typically within 0.3° of the actual solar position, with error attributed to the alignment and leveling of the solar tracker. The solar

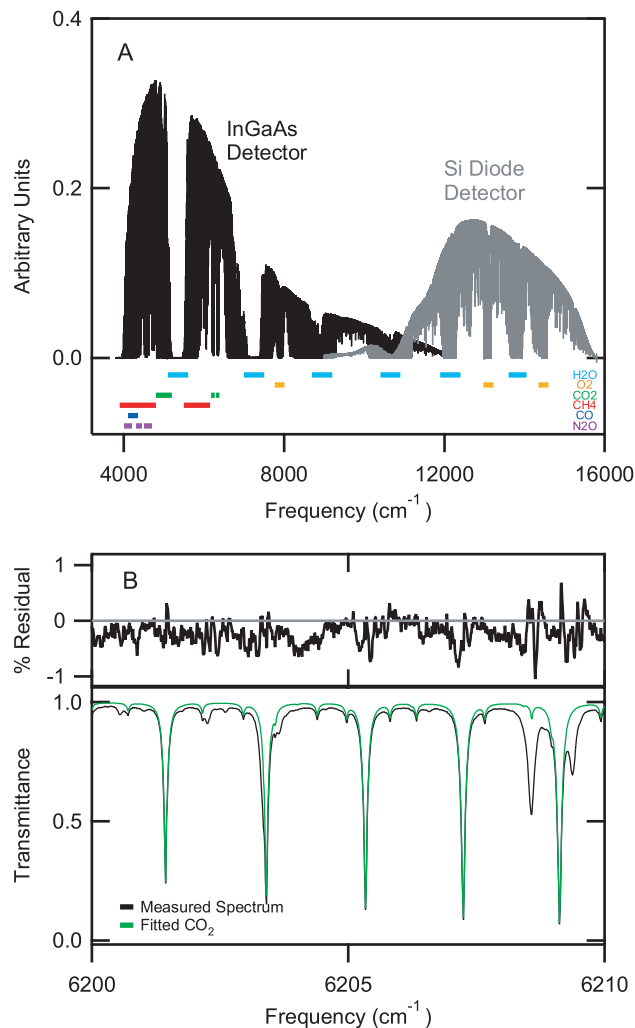


Figure 2.2. (a) A single spectrum recorded on 9 Sep 2004, with 0.014 cm^{-1} resolution. Signal-to-noise ratio is ~ 900 for the InGaAs detector and ~ 500 for the Si diode detector. Near-infrared absorptions by H_2O , O_2 , CO_2 , CH_4 , CO , and N_2O are labeled with color bars. (b) An enlarged view of the same spectrum, demonstrating the resolution and signal-to-noise in a region with strong CO_2 lines.

beam is directed down through a hole in the laboratory roof, which is sealed with an 11.5 cm diameter wedged CaF_2 window. Inside the laboratory, a small fraction of the incoming solar beam is focused onto a Si quadrant detector located at the entrance to the spectrometer. The solar tracker then uses the quadrant detector signal for active tracking of the sun, with a manufacturer-specified tracking accuracy of 0.6 mrad. Three heaters on the base of the solar tracker activate when the temperature drops below 5°C , to prevent damage to the optics and electronics.

The solar tracker is housed in a fiberglass telescope dome, manufactured by Technical Innovations, Inc. in Barnesville, Maryland. The dome is constructed of industrial grade fiberglass, with a $1.0 \text{ m} \times 1.3 \text{ m}$ oval base. The wide shutter opening allows unobstructed views from the horizon to 5° beyond zenith. The dome is bolted to the container roof, which is reinforced with eight 6.4 cm thick steel tubes welded to the frame, and covered with a 0.64 cm thick steel plate. This stabilizes the solar tracker and prevents vibrations that may degrade spectral quality and flexing of the container roof which may degrade the solar tracker alignment.

A Setra Systems, Inc. Model 270 pressure transducer ($\pm 0.3 \text{ hPa}$), is mounted inside the container, with an input tube at $\sim 2 \text{ m}$ outside. Accurate knowledge of the pressure is important for evaluating of the accuracy of the retrieved O_2 columns. In addition, synoptic surface pressure variations of $\pm 10 \text{ hPa}$ ($\pm 1\%$) would overwhelm the changes in the total CO_2 column that we wish to observe. The calibration of the pressure sensor is checked periodically by comparison to a Fortin mercury manometer (Princo Instruments, Model 453) mounted in the laboratory as an absolute standard. In addition, the temperature of the Setra pressure transducer is monitored for evidence of bias. A weather station mounted at $\sim 5 \text{ m}$ includes sensors for air temperature ($\pm 0.3^\circ \text{C}$), relative humidity ($\pm 3\%$), solar radiation ($\pm 5\%$ under daylight spectrum conditions), wind speed ($\pm 0.5 \text{ m s}^{-1}$), wind direction ($\pm 5^\circ$), and the presence of rain.

A small network camera (Stardot Technologies) with a fisheye lens (2.6 mm focal length) is positioned on the roof of the laboratory. The dome, solar tracker, weather station, and a

wide view of the sky are visible within the field of view of the camera. This allows us to remotely monitor the operation of the equipment and verify weather conditions.

Accurate knowledge of the time is critical in calculating the solar zenith angle (SZA), which is necessary to convert retrieved atmospheric slant column abundances into vertical column abundances. We use a high-precision GPS satellite receiver with a network time server (Masterclock NTP100-GPS) to maintain time synchronization of the Bruker 125HR.

2.3.3 Data Acquisition and Instrumental Automation

The laboratory equipment consists of the 125HR spectrometer, scroll pump, solar tracker, dome, weather station, NTP-GPS satellite time receiver, network camera, heaters (for 125HR, solar tracker, and scroll pump), temperature sensors, current and voltage sensors, and uninterruptible power supply (UPS). Each of these components is monitored and/or controlled with an integrated CPU board (Hercules, Diamond Systems) and an additional custom-built control board. The Hercules board includes four serial ports, used for communication with the solar tracker, dome, weather station, and modem. The Hercules board also includes 32 wide-range analog inputs for monitoring temperatures, voltage, currents, and the pressure of the scroll pump. Five digital I/O lines of the Hercules board are used to command power to the solar tracker, dome, modem, FTS, and the FTS reset line. The FTS, network camera, NTP-GPS satellite time receiver, and UPS are IP-addressable and are commanded within the local area network.

The operating system chosen for the Hercules computer is QNX (QNX, Kanata, Ontario), a realtime, multitasking, multiuser, POSIX-compliant operating system for the Intel family of microprocessors. QNX was selected due to its stability and because its simple message-passing method of inter-process communication allows the acquisition and control functions of the data acquisition software to be separated into a number of logically discrete processes.

Throughout the night, the acquisition software records weather and housekeeping data. When the calculated solar elevation angle reaches 0° , the scroll pump is commanded on and the FTS is evacuated to 0.5 hPa. Following the pumping sequence, the dome opens

and the solar tracker points to the calculated solar ephemeris. If the solar intensity is sufficient (45 W m^{-2}), the solar tracker begins active tracking of the sun and the FTS begins acquisition of solar interferograms. The specific acquisition parameters, including the field stop diameter, detector gains, scanner velocity, and optical path difference, are set in software. Typically, each scan requires 110 seconds to complete and consists of a single-sided interferogram with 45 cm optical path difference recorded at 7.5 kHz laser fringe rate. Forward and reverse interferograms (with the moving mirror traveling away from and toward the fixed mirror) are acquired in sequence. Throughout each scan, the solar intensity measured by the solar tracker quadrant sensor is recorded at 0.5 Hz. Since only spectra acquired under stable solar intensity are suitable for atmospheric retrievals, the standard deviation of the solar intensity is later used to evaluate spectral quality. Forward and reverse interferograms are analyzed separately to maximize the number of unobstructed scans. Acquisition of solar interferograms continues as long as the solar intensity is sufficient for active tracking of the sun. If the weather station detects rain, then the dome closes and spectral acquisition ceases until weather conditions improve. When the calculated solar elevation reaches 0° at the end of the day, the dome is closed.

Each night, interferograms recorded during the day are copied onto a removable hard disk. Overnight analysis software performs a Fourier transform to produce spectra from the interferograms, and performs preliminary atmospheric column retrievals. These results are then emailed to Pasadena to monitor performance. At two month intervals, the removable hard disk is manually replaced with an empty one. The full disk is mailed to Pasadena for analysis and archiving. This is necessary because only dial-up internet access is available at the WLEF site. The operational data rate is $\sim 50 \text{ GB month}^{-1}$.

2.4 Measurement Site

The FTS observatory was assembled and tested in Pasadena, California, and deployed to northern Wisconsin during May 2004. The laboratory is located 25 m south of the WLEF television tower site (45.945 N, 90.273 W, 442 m above sea level) in the Chequamegon National Forest, 12 km east of Park Falls, Wisconsin (pop. 2800). The region is heavily forested with low relief, and consists of mixed northern hardwoods, aspen, and wetlands. Boreal lowland and wetland forests surround the immediate research area. The

Chequamegon National Forest was extensively logged between 1860 and 1920, but has since regrown.

This site was chosen because the National Oceanic and Atmospheric Administration Earth Systems Research Laboratory (NOAA ESRL) and other organizations conduct extensive in situ measurements at the WLEF tower, facilitating intercomparison between the column and boundary layer measurements. Monitoring began in October 1994, when WLEF was added as the second site in the Tall Tower program. CO₂ concentrations are measured continuously at six levels on the 447 m tower [Zhao *et al.*, 1997; Bakwin *et al.*, 1995]. Fluxes of CO₂, water vapor, virtual temperature, and momentum are monitored at three levels [Berger *et al.*, 2001; Davis *et al.*, 2003]. In addition, NOAA ESRL conducts weekly flask sampling [Komhyr *et al.*, 1985] and monthly aircraft profiles which collect flask samples between 0.5 km and 4 km [Bakwin *et al.*, 2003].

2.5 Data Analysis

In this work, spectra are analyzed using a non-linear least-squares spectral fitting algorithm (GFIT) developed at the Jet Propulsion Laboratory. Atmospheric absorption coefficients are calculated line-by-line for each gas in a chosen spectral window, and are used together with the assumed temperature, pressure, and VMR profile in the forward model to calculate the atmospheric transmittance spectrum. This is compared with the measured spectrum and the VMR profiles are iteratively scaled to minimize the RMS differences between the calculated and measured spectra. The theoretical instrument lineshape, verified from fits to low-pressure HCl gas cell lines, is used in calculating the forward model. Figure 2.2b shows a measured spectrum and the fitted result, for a region with strong CO₂ lines.

The atmosphere is represented by 70 levels in the forward model calculation. Pressure- and temperature-dependent absorption coefficients are computed for each absorption line at each level. Profiles of temperature and geopotential height are obtained from the NOAA Climate Diagnostics Center (CDC), with 17 pressure levels from 1000 to 10 hPa and 1° × 1° geographic resolution. At pressures less than 10 hPa, climatological profiles of

temperature and geopotential height are used. Measured surface pressure is used to define the lowest model level.

We retrieve CO₂ and O₂ in three bands: O₂ 0–0 $a^1\Delta_g^- X^3\Sigma_g^-$ ($\nu_0 = 7882 \text{ cm}^{-1}$); CO₂ (14°1) – (00°0) ($\nu_0 = 6228 \text{ cm}^{-1}$); and CO₂ (21°2) – (00°0) ($\nu_0 = 6348 \text{ cm}^{-1}$). These will be referred to as the O₂ 7882 cm⁻¹, CO₂ 6228 cm⁻¹, and CO₂ 6348 cm⁻¹ bands. Retrievals in these three bands require accurate spectroscopic parameters for O₂, CO₂, H₂O, and solar lines. The HITRAN 2004 linelist parameters [Rothman *et al.*, 2005] were found to be deficient at the high accuracies that we require. In HITRAN 2004, the O₂ 7882 cm⁻¹ band has severe errors in strengths for low J lines and errors in widths for high J lines; the CO₂ 6228 cm⁻¹ and 6348 cm⁻¹ bands have errors in line positions, air-broadened widths, and pressure shifts.

We have adopted improved line parameters for the O₂ 7882 cm⁻¹ retrievals, including line strengths from PGOPHER model results [Newman *et al.*, 2000], air-broadened widths [Yang *et al.*, 2005], and temperature-dependent air-broadened widths [Yang *et al.*, 2005]. In addition, we have made two empirical corrections to minimize temperature and airmass dependence of the O₂ retrieval: (i) The air-broadened width values [Yang *et al.*, 2005] have been increased by 1.5%. (ii) The temperature-dependence of the air-broadened width values [Yang *et al.*, 2005] have been increased by 10% to bring them into better agreement with measurements by Newman *et al.* [2000]. Both of these empirical corrections are within the reported measurements uncertainties. Four recent laboratory studies report the integrated O¹⁶O¹⁶ 7882 cm⁻¹ band strength as $3.166 \pm 0.069 \times 10^{-24} \text{ cm molecule}^{-1}$ [Lafferty *et al.*, 1998], $3.10 \pm 0.10 \times 10^{-24} \text{ cm molecule}^{-1}$ [Newman *et al.*, 1999] (all O₂ isotopes), $3.247 \pm 0.080 \times 10^{-24} \text{ cm molecule}^{-1}$ [Cheah *et al.*, 2000], and $3.210 \pm 0.015 \times 10^{-24} \text{ cm molecule}^{-1}$ [Newman *et al.*, 2000]. Because the Newman *et al.* [2000] PGOPHER model shows good agreement with our atmospheric fitting retrievals, we have also adopted the Newman *et al.* [2000] integrated band strength.

In addition to the discrete lines of the O₂ 7882 cm⁻¹ band, there is an underlying continuum absorption caused by collision-induced absorption. Based on laboratory measurements [Smith and Newnham, 2000; Smith *et al.*, 2001], we generated a model of collision-induced

absorption which includes separate contributions from O₂-O₂ and O₂-N₂ collisions. Although the collision-induced absorption is included in the line-by-line calculation to improve estimation of the continuum, only the discrete 7882 cm⁻¹ O₂ lines are used in the computation of the O₂ column amount.

We have used updated line parameters for the CO₂ 6228 cm⁻¹ and 6348 cm⁻¹ band line strengths, air-broadened widths, and pressure shifts based on recent work by Bob Toth [*in preparation*, 2006]. We have also adopted updated H₂O line parameters for the 5000 – 7973 cm⁻¹ region [*Toth, private communication*, 2005]. These new linelists were found to give superior spectral fits to our atmospheric spectra. The solar linelist for all near-infrared spectral retrievals is derived from disk-center solar spectra recorded at Kitt Peak (31.9 N, 116 W, 2.07 km).

For O₂, the assumed a priori VMR profiles are constant with altitude. For CO₂, the assumed a priori VMR profiles vary seasonally in approximate agreement to model output from *Olsen and Randerson* [2004]. We have examined the sensitivity of the column CO₂ retrieval to different reasonable a priori functions, including a profile which is constant with altitude, and found that the effect on retrieved column CO₂ is ≤ 0.1%.

2.5.1 Column O₂ and CO₂

The consistency between retrieved column O₂ and measured surface pressure is an important test of instrumental stability. O₂ is well-mixed in the atmosphere, with a dry-air VMR of 0.2095. This provides an internal standard that can be used to check the short-term and long-term precision of the FTS column retrievals. As described in Section 2.3, surface pressure at the Park Falls site is recorded at 1 Hz using a calibrated Setra 270 pressure sensor. The calibrated accuracy of this sensor is ~0.3 mb, which corresponds to an uncertainty of ~0.03% in the surface pressure. For the May 2004 – October 2005 spectra, retrieved column O₂ is consistently $2.27 \pm 0.25\%$ higher than the dry pressure column (where the dry pressure column is equal to the observed surface pressure converted to a column density minus the retrieved H₂O column). This error exceeds both the uncertainty in the dry pressure column and the reported 0.5% uncertainty in the integrated O¹⁶O¹⁶ 7882 cm⁻¹ band strength of 3.21×10^{-24} cm molecule⁻¹ ± 0.015×10^{-24} cm molecule⁻¹ [*Newman et*

al., 2000]. However, the $\sim 4\%$ spread in recent measurements of the integrated $O^{16}O^{16}$ 7882 cm^{-1} band strength (Section 2.4) suggests that this discrepancy may fall within the uncertainty of the laboratory measurements. In this analysis, the retrieved O_2 columns have been reduced by 2.27% to bring the retrievals into agreement with the known atmospheric concentration of O_2 . Figure 2.3a shows O_2 retrievals for airmasses between 2 and 3 (SZA $60 - 70$ deg) plotted as a function of the dry pressure column. Throughout this work, “airmass” refers to the ratio of the slant column to the vertical column and is approximately equal to the secant of the SZA; when the sun is directly overhead, the SZA is 0 deg and the airmass is 1.0. The residuals are shown in the upper panel of Figure 2.3a.

Figure 2.3b shows the time series of O_2 VMR, calculated from column O_2 / dry pressure column. Results are not shown for 8 May 2005 – 14 Jul 2005, due to an instrumental error in solar pointing. Much of the scatter in Figure 2.3b can be attributed to error in the linestrengths and the air-broadened widths that cause the O_2 retrievals to vary with temperature and airmass. However, the systematic increase in O_2 VMR over time ($\sim 0.3\%$) is larger than (and of opposite sign to) the seasonal changes in O_2 VMR. Coincident changes in HCl concentration retrieved from the calibration cell are also observed. During May 2004 – October 2005, the reflectivity of the gold-coated solar tracker mirrors slowly degraded due to a manufacturing flaw. This reduced the measured solar intensity by approximately 60% in the near-infrared spectral region. We believe that the errors observed in the O_2 and HCl retrievals may be caused by this signal loss, coupled with non-linearity in the response of the InGaAs detector. Studies are underway to quantify this error and remove its influence on the retrievals.

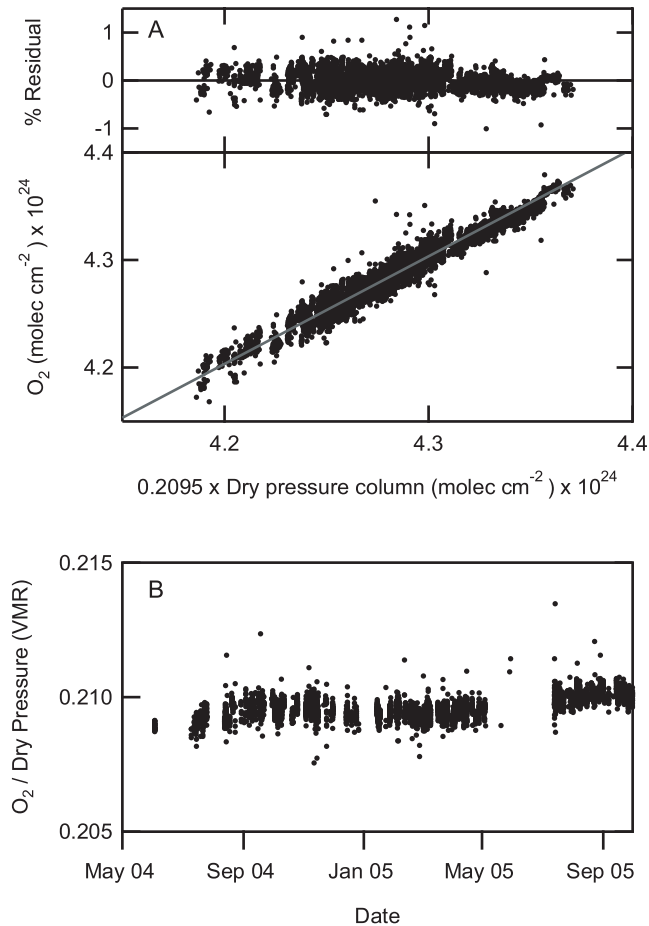


Figure 2.3. (a) Relationship between retrieved column O₂ and dry surface pressure for spectra recorded at airmasses between 2 and 3. The retrieved column O₂ has been reduced by 1.0227. Dry surface pressure is the measured surface pressure converted to a column density minus the retrieved H₂O column. (b) Time series of column-average O₂ VMR during May 2004 – Oct 2005. Scatter is attributed to error in the linestrengths and air-broadened widths which cause the O₂ retrievals to vary with temperature and airmass. The systematic changes of O₂ VMR over time are attributed to detector non-linearity.

Column retrievals of CO₂ from the 6228 cm⁻¹ and 6348 cm⁻¹ bands show high precision and repeatability. Observations of column CO₂ during one clear day and one partly cloudy day in August 2004 are shown in Figure 2.4a. Figure 2.4b shows the column O₂ retrievals during the same time period. Spectra have been discarded as obstructed by clouds if the solar intensity measured by the quadrant detector fluctuated by more than 5% rms during the recording of an interferogram. The mean and standard deviation of the CO₂ columns measured during a one-hour clear observation period around local noon (24 individual spectra) on 14 Aug 2004 is $7.7235 \pm 0.0078 \times 10^{21}$ cm⁻² and $7.7406 \pm 0.0074 \times 10^{21}$ cm⁻² respectively for the 6228 cm⁻¹ and 6348 cm⁻¹ CO₂ bands. This precision of ~0.1% is

typical for column CO₂ obtained under clear sky conditions in Park Falls. However, the 6228 cm⁻¹ and 6348 cm⁻¹ band CO₂ retrievals differ by ~0.2% in absolute column CO₂. This is attributed to errors in spectroscopic parameters for linestrengths and air-broadened linewidths. Observations on 15 Aug 2004 during partly cloudy conditions show greater variability in Figures 2.4a and 2.4b, even after filtering for the standard deviation of the solar radiance to remove spectra that are significantly obstructed by clouds. Column-average CO₂ VMR can be calculated from retrieved CO₂ column, according to

$$(2.1) \quad f_{CO_2, avg} = \frac{column_{CO_2}}{total\ dry\ column}$$

There are two methods for calculating the total dry column:

$$(2.2) \quad total\ dry\ column = \frac{P_s}{m_{air}g} - column_{H_2O}$$

$$(2.3) \quad total\ dry\ column = \frac{column_{O_2}}{0.2095}$$

where P_s is surface pressure, m is molecular mass, and g is gravitational acceleration. In Park Falls, the column H₂O correction in (2.2) is a maximum of 0.6%.

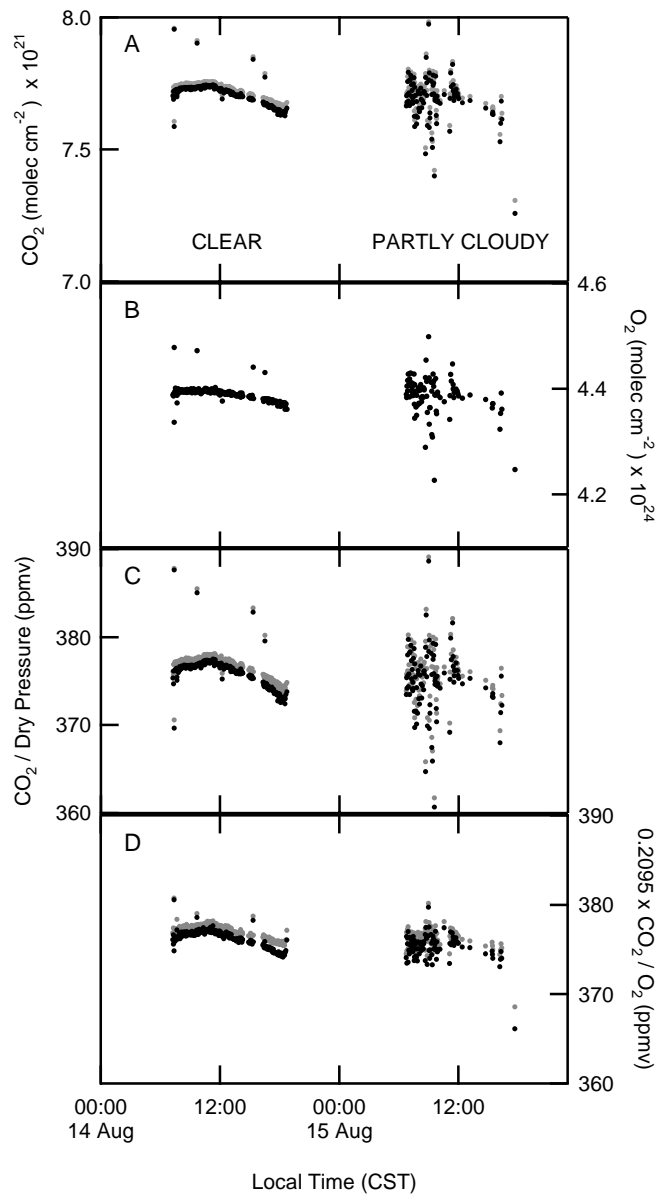


Figure 2.4. Spectral retrievals compared for a clear day (14 Aug 2004) and a partly cloudy day (15 Aug 2004). (a) Column CO_2 retrieved from the 6228 cm^{-1} (black) and 6348 cm^{-1} (gray) bands. Although the retrievals demonstrate precision of $\sim 0.1\%$, there is a systematic offset of $\sim 0.2\%$ between the two bands. This offset is attributed to errors in the CO_2 linelist parameters. (b) Column O_2 retrieved from the 7882 cm^{-1} band. (c) Column-average CO_2 VMR calculated from column CO_2 / dry surface pressure. (d) Column-average CO_2 VMR calculated from $0.2095 \times \text{column } \text{CO}_2 / \text{column } \text{O}_2$.

Using (2.3) will improve the precision of the column-average CO_2 VMR (f_{CO_2}) if scatter in the column abundances is common to both the CO_2 and O_2 . Common scatter could arise from errors in the spectra, such as instrumental lineshape or detector non-linearity, or from

errors in the calculated slant path due to uncertainty in the surface pressure or SZA. However, dividing by column O₂ will increase the random scatter (since column O₂ is typically noisier than P_s) and will introduce spectroscopic linelist errors from the O₂ region, such as temperature- and airmass-dependence, into the column-average CO₂ VMR. In addition, the systematic changes in column O₂ observed over time in Figure 2.3b are likely due to detector non-linearity. However, this systematic error is expected to affect the CO₂ and O₂ column retrievals similarly, and can be eliminated from the column-average CO₂ VMR by using (2.1) and (2.3).

Column-average CO₂ VMR calculated via (2.2) and (2.3) is shown in Figures 2.4c and 2.4d. Comparing Figures 2.4c and 2.4d, the greatest improvement in scatter is seen on the partly cloudy day (15 Aug 2004). The major sources of scatter on cloudy days are error in the solar pointing and variation in intensity during the scan, which affect the CO₂ and O₂ retrievals similarly. Dividing column CO₂ by column O₂, rather than dry pressure column, therefore improves the precision, especially on partly cloudy days. A comparison of the results is shown in Table 2.1.

Table 2.1. Mean and standard deviation of column CO₂ measurements during a one-hour observational period around local noon.

	Column CO ₂ ($\times 10^{21} \text{ cm}^{-2}$)	Column CO ₂ / dry surface pressure (ppmv)	$0.2095 \times$ column CO ₂ / column O ₂ (ppmv)
Clear day (14 Aug 04) 6228 cm ⁻¹ band	7.7235 ± 0.0078	376.46 ± 0.30	376.55 ± 0.26
Clear day (14 Aug 04) 6348 cm ⁻¹ band	7.7406 ± 0.0074	377.29 ± 0.28	377.38 ± 0.22
Cloudy day (15 Aug 04) 6228 cm ⁻¹ band	7.707 ± 0.058	375.8 ± 2.8	375.48 ± 0.82
Cloudy day (15 Aug 04) 6348 cm ⁻¹ band	7.724 ± 0.055	376.7 ± 2.7	376.35 ± 0.68

2.6 Comparison of FTS Column and Integrated Aircraft Profiles

The Intercontinental Chemical Transport Experiment – North America (INTEX-NA) and CO₂ Boundary-layer Regional Airborne Experiment (COBRA) campaigns provided an opportunity to calibrate the column CO₂ measurements on an absolute scale relative to the

standardized network of in situ measurements. As the difference between CO₂ 6228 cm⁻¹ and 6348 cm⁻¹ column retrievals in Figure 2.4a demonstrates, results from each of the CO₂ bands are precise, but not sufficiently accurate. This is attributed to remaining limitations in the available spectroscopic parameters.

The NASA DC-8 and University of Wyoming King Air measured in situ CO₂ during profiles over the WLEF Tall Tower site during summer 2004, using well-calibrated, mature in situ CO₂ sensors. Onboard the DC-8, dry CO₂ VMR was measured at 1 Hz using a modified LI-COR model 6252 infrared gas analyzer [Vay *et al.*, 2003; Anderson *et al.*, 1996]. In-flight calibrations were performed at 15 minute intervals using standards traceable to the WMO Central CO₂ Laboratory. Onboard the King Air, similar 1 Hz measurements were performed using a modified LI-COR model 6251 [Daube *et al.*, 2002]. In-flight calibrations were performed with standards traceable to the Carbon Dioxide Research Group at the Scripps Institute of Oceanography and NOAA ESRL. In-flight calibrations show that the typical long term flight-to-flight precision of this technique is better than ±0.1 ppmv [Daube *et al.*, 2002].

The aircraft CO₂ profiles can be integrated with respect to pressure for direct comparison with FTS column CO₂. Mathematically, this is found by combining the definition of the column integral

$$(2.4) \quad column_{CO_2} = \int_{z_s}^{\infty} f_{CO_2} n dz$$

with the hydrostatic equation

$$(2.5) \quad dz = \frac{-dp}{g m_{air} n}$$

to yield

$$(2.6) \quad column_{CO_2} = \int_0^{P_s} \frac{f_{CO_2}}{gm_{air}} dp$$

where f is the atmospheric mixing ratio, g is gravitational acceleration, m is molecular mass, n is the number density, p is pressure, P_s is surface pressure, z is height, and Z_s is the surface height. The atmospheric mixing ratio of CO_2 is defined as

$$(2.7) \quad f_{CO_2} = f_{CO_2,dry}(1 - f_{H_2O})$$

where $f_{CO_2,dry}$ is the dry-air CO_2 vmr, measured by in-situ instruments. Combining equations (2.6) and (2.7) gives

$$(2.8) \quad column_{CO_2} = \int_0^{P_s} \frac{f_{CO_2,dry}}{gm_{air,dry} \left(1 + \frac{m_{H_2O}}{m_{air,dry}} \left(\frac{f_{H_2O}}{1 - f_{H_2O}} \right) \right)} dp$$

Integrated column CO_2 from (2.8) can be divided by the total column from (2.2) to yield the column-average CO_2 VMR.

Eight unique aircraft profiles were measured on five dates during 2004: 12 Jul, 14 Jul, 15 Jul, 14 Aug, and 15 Aug. The first profile of the series, shown in Figure 2.5a, was a descending spiral by the NASA DC-8 from 10.0 km to 0.7 km. Because the aircraft has a limited altitude range, it is necessary to make assumptions about CO_2 and H_2O in the upper troposphere and stratosphere when using (2.8) to find integrated column CO_2 . The

tropopause pressure is determined from the NOAA CDC assimilated temperature profile. The median CO₂ value measured in the free troposphere is assumed to extend from the aircraft ceiling to the tropopause. Above the tropopause, the assumed CO₂ profile is taken from an in situ balloon profile (35 N, 104 W) recorded over Fort Sumner, New Mexico during September 2004. The balloon profile of CO₂ as a function of altitude is coordinate-transformed into CO₂ as a function of potential temperature (θ), using simultaneous temperature and pressure measurements. For the aircraft profile, θ is calculated from the NOAA CDC assimilated temperature data. CO₂ is assumed to be well-mixed in the planetary boundary layer between the surface and the 0.7 km floor of the aircraft profile. This is confirmed by in situ measurements on the Tall Tower. The CO₂ profile shown in Figure 2.5b is integrated with respect to pressure to find column CO₂. The assumed CO₂ profile above the aircraft ceiling contributes the greatest uncertainty to the integration, and we have attributed a generous uncertainty of ± 2 ppmv to this portion of the profile.

Figure 2.5d shows the FTS column-average CO₂ recorded during a two-hour period which brackets the aircraft profile. These profiles were performed at airmass 1.1 – 2.0 (SZA 25 – 60 deg). The column data is not continuous, because intermittent cloud prevented the acquisition of solar spectra. The 45-minute period of the aircraft profile is indicated. The averaging kernel for the FTS CO₂ retrievals during this period is shown in Figure 2.5c. The shape of the averaging kernel is typical for a uniformly mixed, moderately strong absorber fitted by a non-linear least-squares profile-scaling retrieval. To accurately compare the FTS column-average CO₂ and integrated aircraft profile, it is necessary to weight the aircraft profile by the FTS averaging kernel [*Rodgers and Connor, 2003*]. Because the averaging kernel varies slightly with airmass, a separate averaging kernel is calculated for each aircraft overpass.

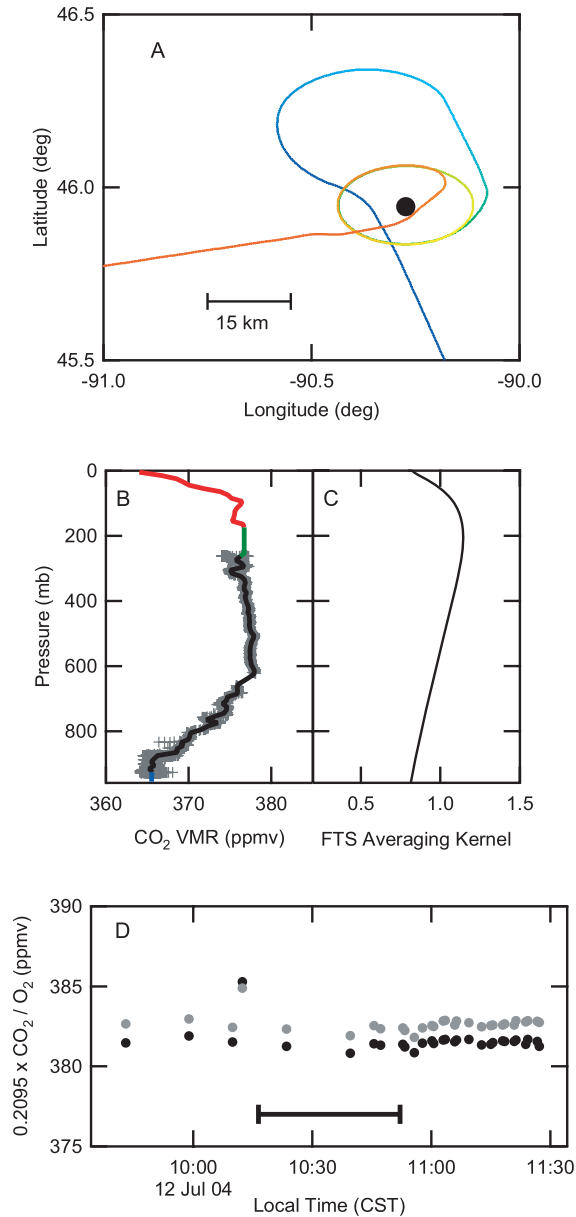


Figure 2.5. (a) Ground track of the NASA DC-8 during a vertical profile from 0.7 – 10.0 km on 12 Jul 2004. The location of the Wisconsin Tall Tower is indicated. Aircraft altitude is shown in color, where red = 0 km and purple = 12 km. (b) In situ CO₂ measured during the 12 Jul 2004 profile. Tropopause pressure is determined from the NOAA CDC reanalysis. Above the aircraft ceiling (10.0 km), the median measured free tropospheric CO₂ value is assumed to extend to the tropopause. Above the tropopause, the assumed CO₂ profile is taken from a Sept 2004 balloon profile from 35 N, 104 W. The CO₂ profile is integrated with respect to pressure to calculate the total column. (c) Averaging kernel for the FTS CO₂ retrievals. (d) Column-averaged CO₂ VMR for FTS spectra recorded during the aircraft profile. CO₂ 6228 cm⁻¹ band retrievals shown in black; CO₂ 6228 cm⁻¹ band retrievals shown in gray. Intermittent clouds prevented continuous data acquisition.

Comparison of the eight integrated aircraft profiles with the FTS CO₂ columns is shown in Figure 2.6. There is a linear relationship between the integrated aircraft columns and the retrieved FTS columns. The slope relationships differ for the two CO₂ bands, with values of 1.0216 and 1.0240 for CO₂ 6228 cm⁻¹ and CO₂ 6348 cm⁻¹ respectively. The standard deviation of the fitting residuals is 0.39 ppmv and 0.42 ppmv for the two bands. The slope relationships from Figure 2.6 can be used to correct the FTS CO₂ columns, bringing them into absolute agreement with the calibrated in situ network.

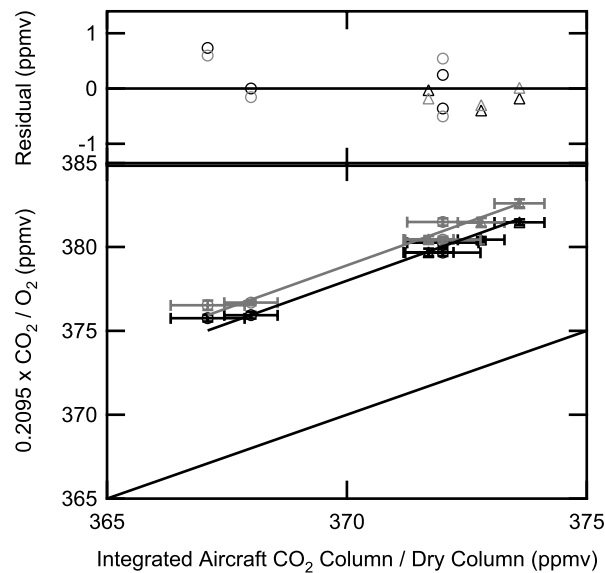


Figure 2.6. Integrated profiles by the DC-8 (triangles) and King Air (circles) compared to FTS retrievals from the two CO₂ bands. CO₂ 6228 cm⁻¹ band retrievals shown in black; CO₂ 6348 cm⁻¹ band retrievals shown in gray. Each integrated aircraft profile has been divided by the dry surface pressure, yielding the familiar units of ppmv. The relationship between integrated profile and FTS column-average CO₂ VMR is linear for each band. A linear fit with intercept 0 gives slopes of 1.0216 for the CO₂ 6228 cm⁻¹ band and 1.0240 for the CO₂ 6348 cm⁻¹ band. The upper panel shows the difference between the FTS measurements and the fitted line.

2.6.1 Error Analysis for Column-Average CO₂ VMR

The column-average CO₂ VMR calculated according to $0.2095 \times \text{column CO}_2 / \text{column O}_2$ is affected by three main sources of error:

1. Measurement precision

As discussed in Section 2.5, the standard deviation of column CO₂ / column O₂ during a one hour period is better than 0.1% under clear sky conditions and ~0.2% under partly cloudy conditions. Repeatability of the measurement is not a significant source of error.

2. Spectroscopic errors

As discussed in Section 2.5, the retrieved O₂ columns were reduced by 2.27% to bring them into agreement with the dry surface pressure. Although this correction falls outside the reported uncertainty of the ¹⁶O¹⁶O 7882 cm⁻¹ integrated band strength, we believe that it is likely attributed to an error in the line strengths or air-broadened width parameters.

The absolute accuracy of the CO₂ retrievals was calibrated by comparison to integrated aircraft profiles, resulting in a correction of 1.0216 and 1.0240 for the CO₂ 6228 cm⁻¹ and 6348 cm⁻¹ bands. The standard deviation of the fitting residuals is 0.39 ppmv and 0.42 ppmv, or approximately 0.1%. The aircraft profiles were performed with the sun at airmass 1.1 – 2.0 (SZA 25 – 60 deg), and the column-average CO₂ VMR is now well-calibrated for these values. However, this does not calibrate the column-average CO₂ VMRs at higher airmass. A 1% change in the air-broadened widths results in a CO₂ VMR change of ~0.2% (±0.8 ppmv) at airmass 3 and ~0.6% (±2.3 ppmv) at airmass 12. These parameters are not sufficiently constrained by current spectroscopic linelists, leaving this as a significant source of systematic error which can be correlated with airmass, time of day, and temperature.

3. Systematic instrumental changes over time

As described in Section 2.5, retrieved O₂ VMR increased by ~0.3% during the observation period. Because this increase is seen for O₂ retrievals from the InGaAs detector in the 7882 cm⁻¹ band, and not for O₂ retrievals from the Si diode detector in the 13095 cm⁻¹ A-band, we believe that this is due to detector nonlinearity and can be corrected. We expect that this error affects the CO₂ and O₂ retrievals similarly, but for now assume that the column CO₂ / column O₂ ratio may also have a systematic error of 0.3% over the observation period.

The measurement precision of $\sim 0.1\%$ under clear sky and $\sim 0.2\%$ under partly cloudy conditions does not affect the accuracy of the measurements. However, spectroscopic errors introduce a systematic bias which depends on airmass. We have calibrated the FTS column retrievals at airmass 1.1 – 2.0 during Jul – Aug 2004, and expect that the absolute accuracy at these airmasses has been maintained within 0.3% throughout the subsequent data record.

2.6.2 Column-Average CO₂ VMR During May 2004 – October 2005

Applying the slope corrections from Section 2.6 allows the FTS column-average CO₂ VMR to be compared directly to in situ CO₂ measurements. Column-average CO₂ VMR, corrected in this manner, is shown in Figure 2.7a, together with in situ CO₂ measurements from 30-m and 396-m on the Tall Tower. The in situ CO₂ measurements are influenced by the diurnal rectifier effect, which is caused by the overnight decrease in the height of the planetary boundary layer. During the day, CO₂ surface fluxes are diluted within a thicker boundary layer, while CO₂ surface fluxes at night are concentrated near the surface. The column-average CO₂ VMR is minimally influenced by the diurnal rectifier effect. Summertime drawdown in CO₂ is observed in both the in situ and column measurements.

The seasonal cycle of column-average CO₂ VMR observed at Park Falls during May 2004 – Oct 2005 is shown as daily averages for airmasses between 2 – 4 (SZA 60 – 75 deg) in Figure 2.7b. In situ CO₂ measurements from the Tall Tower are shown as daily averages between 16:00 – 20:00 UT (10:00 – 14:00 CST). As expected, the variation of CO₂ is muted in the column, as compared to surface measurements, on all timescales. During May 2004 – May 2005, the observed peak-to-peak variation of column-average CO₂ VMR is approximately 13 ppmv, with an average value of 376.2 ppmv. Comparing column-average CO₂ retrievals observed in September and October during 2004 and 2005, we calculate a secular increase of 1.8 ppmv yr^{-1} . After accounting for this, we infer a peak-to-peak seasonal amplitude of 11 ppmv for Park Falls. These results are higher than model results by *Olsen and Randerson* [2004], which predict a mean seasonal column CO₂ amplitude of 7 – 8 ppmv in Wisconsin. This difference could potentially arise from an error in the model predictions, due to uncertainty in the specifications of surface fluxes or errors in the parameterization of mixing. Alternatively, the difference could be caused by

differences between the assumed meteorology and emission inventories included in the MATCH model.

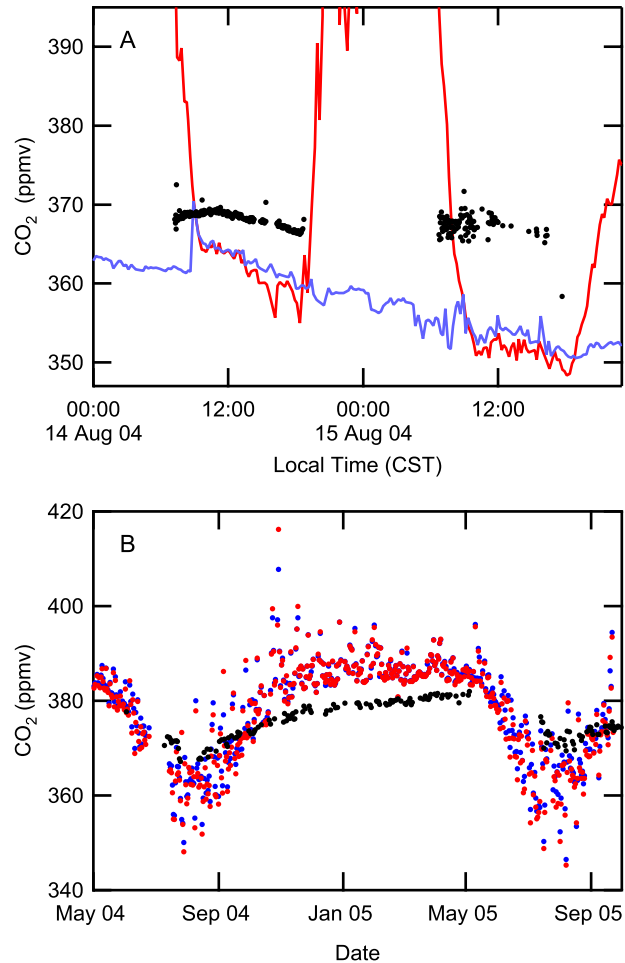


Figure 2.7. (a) Diurnal variation of column-average CO₂ VMR (black) and Tall Tower CO₂ at 30-m (red) and 396-m (blue). (b) Seasonal cycle of column-average CO₂ VMR and Tall Tower CO₂ during May 2004 – Oct 2005. Tall Tower CO₂ is shown as daily averages between 10:00 – 14:00 CST. Column-average CO₂ VMR is shown as daily averages for airmasses 2 – 4 (SZA 60 – 75 deg).

2.6.3 Conclusions

We have deployed an automated solar observatory to Park Falls, Wisconsin. Near-infrared solar absorption spectra have been acquired continuously since May 2004. Short-term and long-term precision are evaluated by the repeatability of column retrievals within a day and by the comparison of column O₂ with surface pressure measurements. The precision of

retrieved column CO₂ under clear-sky conditions is ~0.1%, as determined by the 1 σ variability of retrievals recorded within one hour. Under partly cloudy conditions, the CO₂ column precision is much worse, but can be improved by dividing column CO₂ by column O₂ to calculate column-average CO₂ VMR. This calculation eliminates errors which are common to both CO₂ and O₂ retrievals, such as errors in solar pointing and variation in solar intensity during interferogram acquisition, and allows useful retrievals to be obtained under partly cloudy conditions. Comparison of retrieved column O₂ to dry surface pressure during May 2004 – October 2005 shows linear agreement with a $2.27 \pm 0.25\%$ bias.

The column CO₂ retrievals were calibrated using aircraft profiles from the INTEX-NA and COBRA campaigns during summer 2004. The CO₂ 6228 cm⁻¹ and CO₂ 6348 cm⁻¹ band retrievals over-estimate the integrated aircraft profiles by factors of 1.0216 and 1.0240 respectively, with standard deviation of the fitting residuals of 0.39 ppmv and 0.42 ppmv. The systematic differences are attributed to known uncertainty in the CO₂ spectroscopic linestrengths and air-broadened width parameters. The comparison to aircraft integrated columns allows the CO₂ 6228 cm⁻¹ and CO₂ 6348 cm⁻¹ retrievals to be corrected to the accepted in situ calibration scale. The aircraft profiles were performed with the sun at airmass 1.1 – 2.0, and we are confident that our column-average CO₂ VMRs are now well-calibrated for these summertime, low airmass values. After calibration of the column retrievals with the integrated aircraft profiles and consideration of the complete error budget, we calculate the uncertainty in retrieved column-average CO₂ VMR to be ~0.3% (± 1.1 ppmv) at airmasses less than 2 (SZA less than 60 deg) throughout the measurement timeseries.

2.7 Acknowledgements

We thank Jeffrey Ayers for maintaining the ground-based FTS laboratory in Park Falls, Wisconsin. We thank Arlyn Andrews and the NOAA CCGG for providing WLEF Tall Tower CO₂ measurements. Bruce Daube thanks Victoria Chow and Bhaswar Sen for their support in obtaining the balloon CO₂ profile. We thank Andrew Orr-Ewing for helpful discussions and providing PGOPHER model results for the O₂ 7882 cm⁻¹ band. R.A.W. acknowledges support from the National Science Foundation and the California Institute of Technology. This work was funded by NASA Grant NAG5-12247 and NNG05-GD07G.

Research at the Jet Propulsion Laboratory, California Institute of Technology is performed under contract with NASA.

2.8 References

- Anderson, B. E., G. L. Gregory, J. E. Collins, G. W. Sachse, T. J. Conway, and G. P. Whiting (1996), Airborne observations of spatial and temporal variability of tropospheric carbon dioxide, *J. Geophys. Res.*, *101*, 1985-1997.
- Bakwin, P. S., P. P. Tans, B. B. Stephens, S. C. Wofsy, C. Gerbig, and A. Grainger (2003), Strategies for measurement of atmospheric column means of carbon dioxide from aircraft using discrete sampling, *J. Geophys. Res.*, *108*, doi:10.1029/2002JD003306.
- Bakwin, P. S., P. P. Tans, C. L. Zhao, W. Ussler, and E. Quesnell (1995), Measurements of carbon dioxide on a very tall tower, *Tellus*, *47*, 535-549.
- Berger, B. W., K. J. Davis, C. X. Yi, P. S. Bakwin, and C. L. Zhao (2001), Long-term carbon dioxide fluxes from a very tall tower in a northern forest: Flux measurement methodology, *J. Atmos. Ocean. Tech.*, *18*, 529-542.
- Brault, J. W. (1996), New approach to high-precision Fourier transform spectrometer design, *Appl. Opt.*, *35*, 2891-2896.
- Cheah, S. L., Y. P. Lee, and J. F. Ogilvie (2000), Wavenumbers, strengths, widths and shifts with pressure of lines in four bands of gaseous $^{16}\text{O}_2$ in the systems $a^1\Delta_g - X^3\Sigma_g^-$ and $b^1\Sigma_g^+ - X^3\Sigma_g^-$, *J. Quant. Spectrosc. Radiat. Transfer*, *64*, 467-482.
- Daube, B. C., K. A. Boering, A. E. Andrews, and S. C. Wofsy (2002), A high-precision fast-response airborne CO_2 analyzer for in situ sampling from the surface to the middle stratosphere, *J. Atmos. Ocean. Tech.*, *19*, 1532-1543.
- Davis, K. J., P. S. Bakwin, C. X. Yi, B. W. Berger, C. L. Zhao, R. M. Teclaw, and J. G. Isebrands (2003), The annual cycles of CO_2 and H_2O exchange over a northern mixed forest as observed from a very tall tower, *Glob. Change Biol.*, *9*, 1278-1293.
- Denning, A. S., G. J. Collatz, C. G. Zhang, D. A. Randall, J. A. Berry, P. J. Sellers, G. D. Colello, and D. A. Dazlich (1996), Simulations of terrestrial carbon metabolism and atmospheric CO_2 in a general circulation model: 1. Surface carbon fluxes, *Tellus*, *48*, 521-542.

- Dufour, E., F. M. Breon, and P. Peylin (2004), CO₂ column averaged mixing ratio from inversion of ground-based solar spectra, *J. Geophys. Res.*, *109*, doi:10.1029/2003JD004469.
- GLOBALVIEW-CO₂ (2005), GLOBALVIEW-CO₂: Cooperative Atmospheric Data Integration Project - Carbon Dioxide. CD-ROM, National Oceanic and Atmospheric Administration Climate Monitoring and Diagnostics Laboratory, Boulder, Colorado., edited.
- Gloor, M., S. M. Fan, S. Pacala, and J. Sarmiento (2000), Optimal sampling of the atmosphere for purpose of inverse modeling: A model study, *Glob. Biogeochem. Cy.*, *14*, 407-428.
- Gurney, K. R., R. M. Law, A. S. Denning, P. J. Rayner, D. Baker, P. Bousquet, L. Bruhwiler, Y. H. Chen, P. Ciais, S. Fan, I. Y. Fung, M. Gloor, M. Heimann, K. Higuchi, J. John, T. Maki, S. Maksyutov, K. Masarie, P. Peylin, M. Prather, B. C. Pak, J. Randerson, J. Sarmiento, S. Taguchi, T. Takahashi, and C. W. Yuen (2002), Towards robust regional estimates of CO₂ sources and sinks using atmospheric transport models, *Nature*, *415*, 626-630.
- Komhyr, W. D., R. H. Gammon, T. B. Harris, L. S. Waterman, T. J. Conway, W. R. Taylor, and K. W. Thoning (1985), Global atmospheric CO₂ distribution and variations from 1968-1982 NOAA GMCC CO₂ flask sample data, *J. Geophys. Res.*, *90*, 5567-5596.
- Kurylo, M. J., and S. Solomon (1990), Network for the Detection of Stratospheric Change, NASA Report, Code EEU.
- Lafferty, W. J., A. M. Solodov, C. L. Lugez, and G. T. Fraser (1998), Rotational line strengths and self-pressure-broadening coefficients for the 1.27- μm , $a^1\Delta_g - X^3\Sigma_g^-$, $v = 0-0$ band of O₂, *Appl. Opt.*, *37*, 2264-2270.
- Newman, S. M., I. C. Lane, A. J. Orr-Ewing, D. A. Newnham, and J. Ballard (1999), Integrated absorption intensity and Einstein coefficients for the O₂ $a^1\Delta_g - X^3\Sigma_g^-$ (0,0) transition: A comparison of cavity ringdown and high resolution Fourier transform spectroscopy with a long-path absorption cell, *J. Chem. Phys.*, *110*, 10749-10757.

- Newman, S. M., A. J. Orr-Ewing, D. A. Newnham, and J. Ballard (2000), Temperature and pressure dependence of linewidths and integrated absorption intensities for the $O_2 a^1\Delta_g - X^3\Sigma_g^- (0,0)$ transition, *J. Phys. Chem.*, *104*, 9467-9480.
- Olsen, S. C., and J. T. Randerson (2004), Differences between surface and column atmospheric CO_2 and implications for carbon cycle research, *J. Geophys. Res.*, *109*, doi:10.1029/2003JD003968.
- Rayner, P. J., I. G. Enting, R. J. Francey, and R. Langenfelds (1999), Reconstructing the recent carbon cycle from atmospheric CO_2 , $\delta^{13}C$ and O_2/N_2 observations, *Tellus*, *51*, 213-232.
- Rayner, P. J., and D. M. O'Brien (2001), The utility of remotely sensed CO_2 concentration data in surface source inversions, *Geophys. Res. Lett.*, *28*, 175-178.
- Rodgers, C. D., and B. J. Connor (2003), Intercomparison of remote sounding instruments, *J. Geophys. Res.*, *108*, doi:10.1029/2002JD002299.
- Rothman, L. S., D. Jacquemart, A. Barbe, D. C. Benner, M. Birk, L. R. Brown, M. R. Carleer, C. Chackerian, K. Chance, L. H. Coudert, V. Dana, V. M. Devi, J. M. Flaud, R. R. Gamache, A. Goldman, J. M. Hartmann, K. W. Jucks, A. G. Maki, J. Y. Mandin, S. T. Massie, J. Orphal, A. Perrin, C. P. Rinsland, M. A. H. Smith, J. Tennyson, R. N. Tolchenov, R. A. Toth, J. Vander Auwera, P. Varanasi, and G. Wagner (2005), The HITRAN 2004 molecular spectroscopic database, *J. Quant. Spectrosc. Radiat. Transfer*, *96*, 139-204.
- Smith, K. M., and D. A. Newnham (2000), Near-infrared absorption cross sections and integrated absorption intensities of molecular oxygen (O_2 , O_2-O_2 , and O_2-N_2), *J. Geophys. Res.*, *105*, 7383-7396.
- Smith, K. M., D. A. Newnham, and R. G. Williams (2001), Collision-induced absorption of solar radiation in the atmosphere by molecular oxygen at 1.27 μm : Field observations and model calculations, *J. Geophys. Res.*, *106*, 7541-7552.
- Tans, P. P., I. Y. Fung, and T. Takahashi (1990), Observational Constraints on the Global Atmospheric CO_2 Budget, *Science*, *247*, 1431-1438.
- Vay, S. A., J. H. Woo, B. E. Anderson, K. L. Thornhill, D. R. Blake, D. J. Westberg, C. M. Kiley, M. A. Avery, G. W. Sachse, D. G. Streets, Y. Tsutsumi, and S. R. Nolf (2003),

- Influence of regional-scale anthropogenic emissions on CO₂ distributions over the western North Pacific, *J. Geophys. Res.*, *108*, doi:10.1029/2002JD003094.
- Warneke, T., Z. Yang, S. Olsen, S. Korner, J. Notholt, G. C. Toon, V. Velazco, A. Schulz, and O. Schrems (2005), Seasonal and latitudinal variations of column averaged volume-mixing ratios of atmospheric CO₂, *Geophys. Res. Lett.*, *32*, doi:10.1029/2004GL021597.
- Yang, Z., P. O. Wennberg, R. P. Cageao, T. J. Pongetti, G. C. Toon, and S. P. Sander (2005), Ground-based photon path measurements from solar absorption spectra of the O₂ A-band, *J. Quant. Spectrosc. Radiat. Transfer*, *90*, 309-321.
- Yang, Z. H., G. C. Toon, J. S. Margolis, and P. O. Wennberg (2002), Atmospheric CO₂ retrieved from ground-based near IR solar spectra, *Geophys. Res. Lett.*, *29*, doi:10.1029/2001GL014537.
- Zhao, C. L., P. S. Bakwin, and P. P. Tans (1997), A design for unattended monitoring of carbon dioxide on a very tall tower, *J. Atmos. Ocean. Tech.*, *14*, 1139-1145.

Chapter 3

SURFACE EXCHANGE OF CO₂ OBSERVED BY COINCIDENT EDDY COVARIANCE FLUX AND COLUMN MEASUREMENTS*

3.1 Abstract

Measurements of column CO₂ at the WLEF Tall Tower site in Northern Wisconsin are used to calculate CO₂ exchange on seasonal and daily timescales. Comparisons of column and in situ measurements confirm model predictions that the column measurements are representative of Northern Hemispheric CO₂ exchange over seasonal timescales. TransCom 3 models underpredict the seasonal cycle observed in the column measurements, suggesting that the Carnegie-Ames-Stanford Approach (CASA) terrestrial biosphere model may underestimate the magnitude of the growing season net flux. The precision of the column measurements (~0.1%) is sufficient to directly infer daytime fluxes from the temporal gradient of the CO₂ column. Net ecosystem exchange is calculated from the column abundance of CO₂ and compared with eddy covariance measurements. Although the observation of net ecosystem exchange in the column is obscured by concentration changes due to transport, the column and eddy covariance measurements agree when averaged seasonally.

3.2 Introduction

The atmospheric abundance of CO₂ has increased from 280 ppmv in pre-industrial times to ~370 ppmv in 1999, and continues to increase at a rate of 1 – 2 ppmv yr⁻¹ [*IPCC*, 2001]. This increase is attributed to fossil fuel consumption [*Marland*, 2000] and land use change [*Houghton*, 1999]. The magnitude of the global release of CO₂ from the burning of fossil fuels is well known [*Marland*, 2000]. The discrepancy between this value and the mass of CO₂ accumulating in the atmosphere is attributed to uptake by oceans and the terrestrial biosphere [*Battle et al.*, 2000; *Keeling et al.*, 1993; *Keeling and Shertz*, 1992].

Understanding the current and future carbon balance of the terrestrial biosphere is important for predicting future atmospheric CO₂ levels.

Top-down estimates of the magnitude of CO₂ sources and sinks are currently inferred from in situ measurements at two global networks of surface sites, operated by NOAA and the Scripps Institute of Oceanography [*GLOBALVIEW-CO2*, 2005; *Conway et al.*, 1994; *Keeling et al.*, 1995]. Studies combine these in situ measurements with global transport models to estimate regional-scale surface exchange of CO₂ using inversion techniques [*Gurney et al.*, 2002; *Rayner et al.*, 1999; *Tans et al.*, 1990]. This has proven difficult, because although the measurements are highly accurate, they have limited spatial coverage and are generally confined to the convective boundary layer. Because CO₂ exchange and changes in boundary layer height are correlated on diurnal and seasonal timescales, errors in parameterization of diurnal and seasonal CO₂ fluxes can be aliased into the inferred exchange terms as “rectifier effects” [Denning et al., 1996a; Denning et al., 1995; Denning et al., 1996b].

Integrated column measurements of CO₂ have the potential to constrain top-down estimates of carbon exchange. Because the column integral of CO₂ is not influenced by diurnal variations in the convective boundary layer, column measurements are not affected by the seasonal and diurnal rectifier effect. In addition, column measurements sample a larger portion of the atmosphere, which results in less spatial variability and less influence of local sources and sinks, while retaining information about the regional surface fluxes. Olsen and Randerson [2004] concluded that with a few high-precision observation sites, it would be possible to assess the strength of the Northern Hemisphere carbon sink and that this approach would be less sensitive to model representations of vertical mixing. Similarly, Rayner and O’Brien [2001] observe that column-integrated data are less susceptible than surface measurements to uncertainties in model transport.

Column measurements also have the potential to directly constrain bottom-up estimates of CO₂ exchange on diurnal timescales. Many of the same advantages that make the CO₂ column a useful tool for atmospheric inversions, such as insensitivity to the rectifier effect, also make it useful for directly quantifying regional CO₂ exchange. However, because the

fluxes are inferred from the temporal gradient in the CO₂ column, the column observations must be highly precise. In addition, if changes in the column due to simple transport are not sufficiently small or sufficiently well constrained, they will overwhelm the small changes due to surface uptake.

The potential for column measurements to constrain both top-down and bottom-up estimates of CO₂ exchange is possible because the measurements simultaneously represent two different spatial footprints, when considered over different time scales. The “footprint” is defined as the contribution of each element of the upwind surface area to the measured flux, and is synonymous with the transfer function or source weighting function. Assuming a mean windspeed of 10 m s⁻¹ in the atmospheric boundary layer and free troposphere, the change in column CO₂ within a single 10-hr period represents a footprint length of ~360 km. Observations of daytime changes in CO₂ can be used directly to infer fluxes for this spatial region. Rapid mixing within the troposphere results in a much larger footprint over longer timescales. The seasonal phase and amplitude of a column CO₂ measurement is approximately representative of the entire hemisphere, and model predictions show that the seasonal amplitude of column CO₂ will be similar at terrestrial and oceanic sites within the same latitude band [*Olsen and Randerson, 2004*]. Overall, column measurements will observe the hemispheric seasonal cycle, with daytime changes due to local sources and sinks superimposed on the larger trend.

This work presents CO₂ exchange on seasonal and daily timescales observed by column measurements at a forested site in Northern Wisconsin. Near-infrared solar absorption spectra can be used to determine the column abundance of CO₂ and other greenhouse gases [*Yang et al., 2002; Washenfelder et al., 2006; Dufour et al., 2004; Warneke et al., 2005*]. To evaluate carbon exchange on seasonal timescales, CO₂ column measurements from May 2004 – March 2006 are compared to in situ measurements and TransCom model predictions. To examine carbon exchange on daily timescales, we compare column measurements to eddy covariance measurements acquired in and above the convective boundary layer. We calculate the daytime drawdown of CO₂ observed by column and eddy covariance measurements during short time periods (on the order of six hours) to evaluate

the spatial representativeness of these two datasets in observing CO₂ net ecosystem exchange (NEE).

3.3 Column Measurements: Instrumentation and Data Analysis

The column measurements described in this work were acquired at an automated observatory located at the WLEF Tall Tower site in Northern Wisconsin. The observatory was developed for highly precise, ground-based solar absorption spectrometry, and it is the first dedicated observatory in the Total Carbon Column Observing Network (TCCON). Solar tracking optics and a Fourier Transform Spectrometer (FTS) are used to record near-infrared spectra of the sun at high spectral resolution. Solar spectra are acquired continuously during clear sky conditions, with each spectrum requiring ~110 seconds. Details regarding the FTS observatory and analysis technique can be found in Washenfelder et al. [2006]. Measurement precision of ~0.1% is demonstrated for retrievals of column CO₂ and column O₂ under clear-sky conditions [*Washenfelder et al.*, 2006]. Column-average CO₂ VMRs are calculated by ratioing column CO₂ with surface pressure or column O₂. Column-average CO₂ VMRs have been calibrated by comparison with integrated aircraft profiles [*Washenfelder et al.*, 2006].

3.4 Research Site

The FTS observatory is located 25 m south of the WLEF television tower (45.495 N, 90.273 W, 442 m) in the Park Falls Ranger District of the Chequamegon National Forest, 12 km east of Park Falls, Wisconsin, U.S.A. The Chequamegon National Forest was extensively logged between 1860 and 1920, but has since regrown [*Bakwin et al.*, 1998]. The Wisconsin Department of Natural Resources has employed LANDSAT Thematic Mapper satellite imagery and ground truthing to assemble the Wisconsin Initiative for Statewide Cooperation on Landscape Analysis and Data (WISCLAND) land cover map [*WiDNR*, 1998]. The WISCLAND inventory shows that within a 10-km radius of WLEF, 82.4% of the landcover is classified as aspen, maple, sugar maple, and mixed deciduous and coniferous forests, with an additional 1.4% classified as emergent and wetland meadow, and 2.4% classified as open water. The deciduous species include aspen, birch, maple, basswood, and alder. The coniferous species include balsam fir, red pine, jack pine,

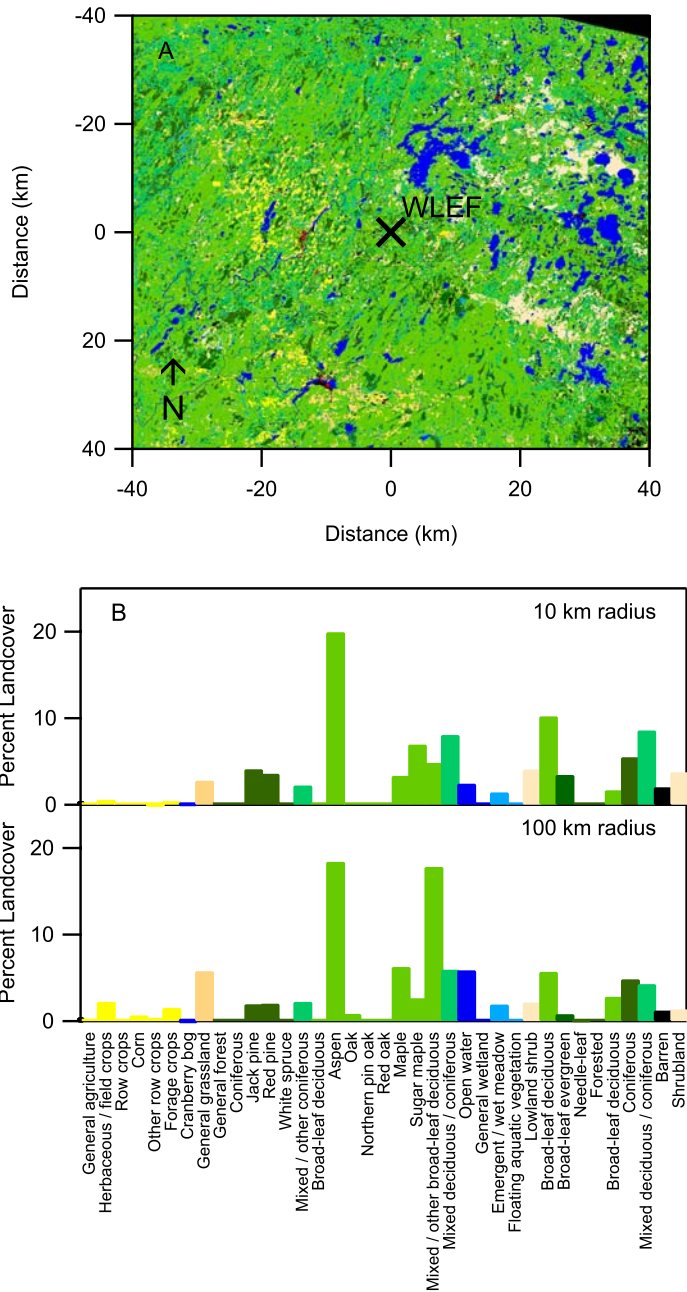


Figure 3.1. (a) Wisconsin Initiative for Statewide Cooperation on Landscape Analysis and Data (WISCLAND) land cover classification map for the region surrounding the WLEF tower site [WiDNR, 1998]. (b) Landcover distribution within a 10-km and 100-km radius of the WLEF tower, demonstrating that the forest cover is roughly homogeneous.

black spruce, and white cedar. Within a 100-km radius of WLEF, 76.6% of the landcover is similarly classified as aspen, oak, maple, sugar maple, and mixed deciduous and coniferous forests, with 1.9% classified as emergent and wetland meadow, and 5.9%

classified as open water. Figure 3.1 shows a map of the study area and a histogram of the WISCLAND landcover designations. Further details regarding landcover are given in the literature [Burrows *et al.*, 2002; Cook *et al.*, 2004; Davis *et al.*, 2003; MacKay *et al.*, 2002].

3.5 Seasonal CO₂ Exchange

3.5.1 Park Falls WLEF Site During 2004 – 2005

Column-average CO₂ VMRs are shown together with in situ CO₂ VMRs recorded at 396-m on the WLEF tower in Figure 3.2. Qualitatively, column CO₂ behaves similarly to surface CO₂, but is much more uniform spatially and temporally [Olsen and Randerson, 2004]. Daytime averages for the column-average CO₂ measurements are calculated for solar zenith angles (SZA) 60 deg – 75 deg (airmass 2 – 4) to minimize seasonal biases due to SZA [see Washenfelder *et al.*, 2006]. Daytime averages for the in situ measurements are shown for 10:00 – 14:00 local standard time, to minimize seasonal bias due to the rectifier effect. The column-average CO₂ VMR is greater than the in situ mixing ratio at the top of the tower during the summer and fall, but less in the winter and spring. This is consistent with model predictions by Olsen and Randerson [2004] for column and surface measurements at Northern Hemisphere mid-latitudes.

During May 2004 – March 2006, the observed peak-to-peak variation of column-average CO₂ at Park Falls is approximately 13 ppmv with an average value of 376.3 ppmv. With a secular trend of 1.8 ppmv yr⁻¹ observed in the column measurements, we infer a peak-to-peak seasonal amplitude of 11 ppmv. This supports the prediction that column measurements in the Northern Hemisphere will be generally representative of Northern Hemispheric CO₂ exchange over seasonal timescales [Olsen and Randerson, 2004]. Column measurements are acquired only under clear-sky conditions, and recent work shows that this may introduce a difference of -0.2 to -0.4 ppmv compared to measurements under all viewing conditions [Corbin and Denning, 2006]. The difference is predicted during both summer and winter and is attributed to enhanced photosynthesis and changes in advection during clear days. Considering this, we report the peak-to-peak seasonal amplitude as 11 ppmv ± 1 ppmv.

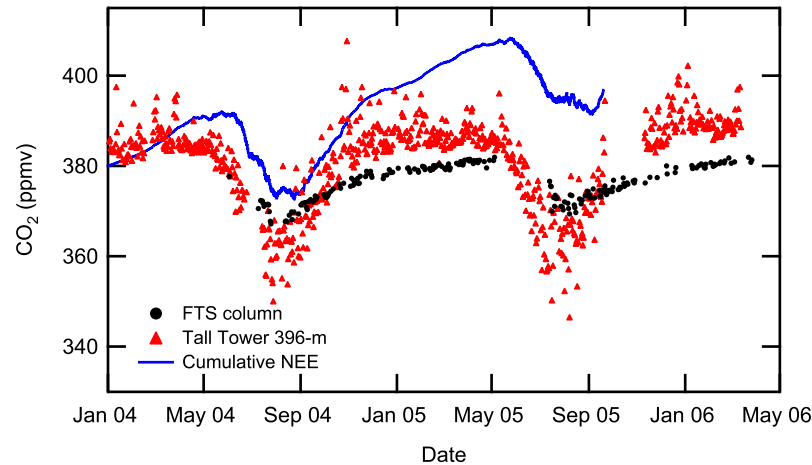


Figure 3.2. CO₂ and surface exchange observed at the WLEF Tall Tower site. Three independent datasets acquired at the WLEF Tall Tower site during 2004 – 2006 are shown. (i) Column-average CO₂ measured by FTS (black; daily average for SZA 60 – 75 deg); (ii) In situ CO₂ VMR at 396-m (red; daily average for 10:00 – 14:00 local standard time); (iii) Cumulative NEE (blue; gap-filled measurements of preferred NEE with constant offset of 380 ppmv).

The observed peak-to-peak seasonal amplitude at Park Falls is similar to the reported amplitude of 11 ppmv observed at Spitsbergen, Norway (78.9 N, 11.9 E, 0.02 km above sea level) during 2002 – 2004 [Warneke *et al.*, 2005] and larger than the reported peak-to-peak seasonal amplitude of ~7 ppmv observed at the Kitt Peak National Solar Observatory (31.9 N, 111.6 W, 2.09 km above sea level) during 1977 – 1995 [Yang *et al.*, 2002]. However, it is difficult to draw further conclusions directly from comparing the seasonal amplitude at Park Falls, Spitsbergen, and Kitt Peak. As a mountain site, Kitt Peak is affected by convective mixing that may vary diurnally and seasonally. Wintertime measurements at Spitsbergen are recorded at high SZA, and this may introduce a seasonal bias of a few ppmv, which has not yet been calibrated.

3.5.2 Comparison to TransCom Model Predictions

The Atmospheric Tracer Transport Model Intercomparison Project (TransCom) is an intercomparison of transport models used to calculate the size and distribution of regional carbon fluxes by inverting in situ measurements. The TransCom 3 experiment included 16 different transport model and model variants that differ in spatial resolution, advection scheme, driving winds, and sub-grid scale parameterizations [Gurney *et al.*, 2002; Gurney

et al., 2003]. For the TransCom 3 comparison, these transport models were initialized identically with a standard set of background fluxes that included fossil fuel emission fields, an annually-balanced terrestrial biosphere, and air-sea gas exchange [Gurney *et al.*, 2002; Gurney *et al.*, 2003]. The seasonal biosphere exchange (1 deg x 1 deg) was derived from the Carnegie-Ames-Stanford Approach (CASA) terrestrial biosphere model [Randerson *et al.*, 1997], and has an annual total flux of zero at every grid cell. The background fossil fuel fluxes were prescribed without seasonality. In the current work, we have adopted the TransCom 3 experimental protocol, but have scaled the 1995 fossil fuel emission inventory by 1.10 to better represent 2004 – 2006.

The TransCom 3 model predictions of the CO₂ seasonal cycle for the 925 mb pressure surface and the total column at the WLEF site are shown in Figure 3.3. Horizontal resolution varies between the models, but is typically on the order of 3 deg × 3 deg. Because the total atmospheric mass of CO₂ in the different models is essentially identical, the range in the model prediction is mainly due to differences in the assumed meteorological wind fields and the representation of atmospheric mixing processes, such as convection. The observed seasonal amplitude in the column significantly exceeds both the average TransCom model prediction and the range of predictions, suggesting that the error is not due to transport.

Yang *et al.* [2006, *in preparation*] analyze the TransCom models together with aircraft profiles, and conclude that (i) the models do not accurately represent the mixing of the planetary boundary layer with the free troposphere (on average they are too stratified); and (ii) a small number of additional measurements in the free troposphere could constrain the models, resulting in more accurate partitioning of inter-hemispheric carbon fluxes. The column measurements provide additional diagnostic information for evaluating the TransCom models. Although they lack the profile information that is available from aircraft measurements, the column measurements are recorded continuously at higher sampling frequency and have a larger seasonal footprint than the aircraft measurements.

The evidence in Figure 3.3 and the mid-tropospheric aircraft data analyzed by Yang *et al.* [2006, *in preparation*] consistently suggests that vertical mixing is under-represented in the

TransCom models. This explanation would also resolve differences between the measured and modeled seasonal cycle of column CO_2 at the Kitt Peak National Solar Observatory [Olsen and Randerson, 2004]. Because the TransCom 3 models are able to reproduce measurements of surface CO_2 , while underestimating the vertical mixing, this suggests that the seasonal variation of NEE in the Northern Hemisphere is underestimated by the CASA neutral biosphere.

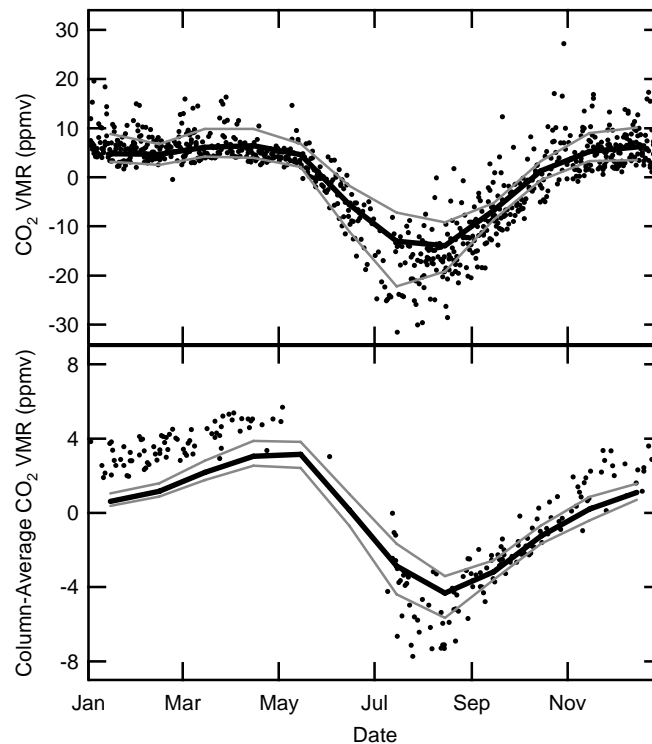


Figure 3.3. (a) TransCom model results for the 925 mb pressure level for the gridbox containing the WLEF Tall Tower site (solid line represents average; grey lines show range of model predictions). Detrended in situ CO_2 VMR measurements from 396-m (daily average for 10:00 – 14:00 local standard time) are also shown (black circles). The trend and annual mean have been subtracted from each dataset. (b) Column-average CO_2 VMRs (black circles) for May 2004 – March 2006 are shown with integrated TransCom vertical profiles (solid line represents average; grey lines show range of model predictions). Each of the TransCom models underpredict the seasonal cycle observed in the column measurements.

3.6 Local CO_2 Exchange

3.6.1 Bottom-Up Estimates of Local CO_2 Exchange.

In contrast to the top-down approach of atmospheric inversions, the bottom-up approach attempts to scale-up direct measurements of CO_2 exchange on local scales to constrain the

global carbon budget. Here, we evaluate the potential of column measurements at the WLEF site for constraining estimates of local NEE and compare these measurements to eddy covariance measurements recorded on the WLEF tower. The main challenge in inferring fluxes from a concentration gradient is that this requires that the column changes due to transport are either small or can be modeled. An additional impediment is that the column measurements are only possible when the sun is unobscured by clouds, meaning that continuous measurements are not available.

Eddy covariance measurements have been used successfully to quantify CO₂ exchange on local scales. The eddy covariance method is a statistical technique used to analyze high frequency wind and scalar atmospheric data to determine the vertical flux of trace gases [Baldocchi, 2003]. The eddy covariance method provides a direct measure of CO₂ surface exchange, and allows NEE to be assessed at the level of an entire ecosystem over timescales of hours to years [Baldocchi *et al.*, 1988; Goulden *et al.*, 1996; Wofsy *et al.*, 1993]. The footprint length is typically 10 – 100 times greater than the measurement height and varies with meteorological conditions, falling in the range of hundreds of meters to tens of kilometers depending on the height of the tower. The method is most applicable over flat terrain, under steady environmental conditions, and with homogeneous vegetation for an extended distance upwind. Ignoring these constraints can introduce systematic errors in interpretation. In addition, diurnal changes in footprint area can introduce difficulty in calculating temporally-integrated NEE [Wang, 2005].

Understanding the spatial representativeness of eddy covariance measurements is a challenge. Measured fluxes may not be broadly representative of different ecosystem classifications due to differences in canopy age, canopy density, tree roots, soil, litter quality, plant species, micrometeorological conditions, and other biological factors [Wang, 2005]. A recent study by Wang [2005] of eddy covariance observations in and around Park Falls shows that a simple ecosystem classification system cannot capture the variability of CO₂ NEE between different ecosystems. Wang concludes that no small flux tower can accurately represent regional CO₂ exchange [Wang, 2005].

3.6.2 Eddy Covariance: Instrumentation and Data Analysis

Fluxes of CO₂, water vapor, virtual temperature, and momentum are measured continuously at 30, 122, and 396 m on the WLEF tower. CO₂ and water vapor mixing ratios are measured using infrared gas analyzers (Li-Cor Inc., Lincoln, Nebraska, model LI-6262). Virtual temperature and momentum are measured using sonic anemometers (Applied Technologies Inc., Boulder, Colorado, model SATI/3K or Campbell Scientific Inc., Logan, Utah, model CSAT3). High-precision, high-accuracy CO₂ mixing ratio measurements are simultaneously recorded at 11, 30, 76, 122, 244, and 396 m using two Li-Cor model LI-6251 infrared gas analyzers [Bakwin *et al.*, 1998; Zhao *et al.*, 1997]. These measurements are used to calibrate the fast-response infrared gas analyzers and to calculate the rate of change of storage for CO₂ [Davis *et al.*, 2003]. The eddy covariance instrumentation and methodology is described in detail in Berger *et al.* [2001] and Davis *et al.* [2003].

NEE is the net flux of carbon from the surface and can be described as the sum of the turbulent flux at the measured height plus the rate of change of CO₂ mass in the atmosphere below. Studies conducted at the WLEF site conclude that the horizontal and vertical advection terms make a negligible contribution to daytime NEE [Wang *et al.*, 2005; Yi *et al.*, 2000]. Previous work has examined the long-term average of NEE at the three observation levels of the WLEF tower [Davis *et al.*, 2003], with consideration of the measurement footprint under varying conditions of convective mixing. The authors developed an algorithm for “preferred” NEE that combines measurements at the three levels to maintain a large footprint while avoiding the influence of the clearing around the tower. Preferred NEE has been adopted for this comparison.

3.6.3 Calculation of Net Ecosystem Exchange from the Total Column

Column and eddy covariance measurements of CO₂ can each be used to calculate NEE. However, the total observed change in the column CO₂ abundance includes changes due to NEE, surface pressure, and transport (horizontal advection in the convective boundary layer and free troposphere). Transport will alter the vertical column of CO₂ if regional gradients exist in the concentration field.

A mathematical expression for NEE can be derived by first considering the vertical column of CO₂, which is defined as

$$(3.1) \quad VC_{CO_2} = \int_{z_s}^{\infty} f_{CO_2} n dz$$

where VC is the vertical column, f_{CO_2} is the volume mixing ratio of CO₂, n is number density, z is height, and Z_s represents the surface altitude. This expression can be combined with the hydrostatic equation

$$(3.2) \quad dz = \frac{-dp}{gm_{air}n}$$

to yield

$$(3.3) \quad VC_{CO_2} = \int_0^{P_s} \frac{f_{CO_2}}{gm_{air}} dp = \frac{\overline{f_{CO_2}} P_s}{gm_{air}}$$

where g is gravitational acceleration, m_{air} is the mean molecular mass, p is pressure, and P_s is surface pressure. Equation 3.3 assumes that g and m_{air} do not vary with pressure, and that f_{CO_2} may be represented by its pressure-weighted column-average value. Next, we differentiate the vertical column with respect to time. The chain rule is employed because both P_s and f_{CO_2} are functions of time.

$$(3.4) \quad \frac{dVC_{CO_2}}{dt} = \frac{VC_{CO_2}}{P_s} \frac{dP_s}{dt} + \frac{VC_{CO_2}}{\overline{f_{CO_2}}} \frac{d\overline{f_{CO_2}}}{dt}$$

Equation 3.4 can be further simplified by introducing the vertical column of O₂, which the FTS observes simultaneously in the near-infrared solar spectra. O₂ is well-mixed in the atmosphere, with a dry-air volume mixing ratio of 0.2095. The vertical column of O₂ can be expressed as

$$(3.5) \quad VC_{O_2} = \frac{\overline{f_{O_2}} P_s}{gm_{air}}$$

Substituting Equations 3.3 and 3.5 into Equation 3.4 gives a complete expression for the observed change in VC_{CO_2} with time, which includes contributions from NEE, change in surface pressure, and transport:

$$(3.6) \quad \frac{dVC_{CO_2}}{dt} - \frac{\overline{f_{CO_2}}}{\overline{f_{O_2}}} \frac{dVC_{O_2}}{dt} = \frac{VC_{O_2}}{\overline{f_{O_2}}} \frac{d\overline{f_{CO_2}}}{dt}$$

The first term on the LHS of Equation 3.6 represents the total observed change in the column. The second term on the LHS of Equation 3.6 represents the change in VC_{CO_2} due to changes in the surface pressure, with the assumption that the change in f_{CO_2} is negligible with respect to the change in surface pressure. The change in column CO₂ due to surface pressure is typically negative during the day, due to the diurnal and semidiurnal pressure tides. The tides have annually-averaged magnitudes of 0.5 hPa and 0.4 hPa respectively, with peaks at ~10:00 and ~9:00/21:00 local standard time [Dai and Wang, 1999]. The RHS represents the change in VC_{CO_2} due to both NEE and transport. It is difficult to

separate these two contributions, because they both alter the observed volume mixing ratio of CO₂.

Quantifying the change in CO₂ due to transport in order to better calculate NEE represents a challenge. Constraining this term would require a model capable of predicting regional CO₂ gradients of less than 1 ppmv over times scales of a many hours. Alternatively, a tracer approach could be used to determine when the influence of transport is negligible. CO is anthropogenic, with a moderate lifetime, no local flux, and a summertime latitudinal gradient. However, we have found that the change in column CO is not well-correlated with changes in column CO₂ due to transport, which precludes the use of CO as a tracer. In general, we expect that the change in V_{CO_2} due to transport is negligible when Equation 3.6 is employed over time periods of a few hours, but that this contribution becomes significant over longer time periods. This work analyzes CO₂ exchange on timescales sufficiently short that transport may be neglected.

Although the precision of column CO₂ retrievals is high, we observe systematic errors that depend on SZA. As the observed optical path through the atmosphere increases with increasing SZA, the optical depth of CO₂ absorption lines increases. The error is attributed to uncertainties in the spectroscopic linelist parameters used to calculate the absorption coefficients. SZA-dependent errors can be introduced by errors in the air-broadened linewidths, the temperature-dependence of the air-broadened linewidths, or the relative strengths of lines with different lower state energies. A small change in the linelist parameters, such as a 1% change in the air-broadened linewidths, will change column-average CO₂ VMR by ± 0.4 ppmv at SZA 70 deg. Unfortunately, the existing laboratory spectroscopy is insufficient to achieve our desired accuracy, and the aircraft profiles previously used for calibration [*Washenfelder et al.*, 2006] were not recorded during high SZAs and can not be used to quantify this error.

For the analysis described in this work, we calculate Equation 3.6 symmetrically around local solar noon (e.g. from [local solar noon - 2] hrs to [local solar noon + 2 hrs]). This eliminates bias due to errors that depend on solar zenith angle, including most spectroscopic errors.

3.6.4 Comparison of Drawdown Observed by FTS and Eddy Covariance

Figure 3.4 shows the drawdown observed during a sunny period in September 2004. The plot shows eddy covariance measurements of NEE and FTS total column measurements corrected by the surface pressure change (Equation 3.6), which represent changes in column CO_2 due to both NEE and transport. In each case, the measurements have been integrated with respect to time, and the noontime average has been subtracted from each 24-hour period of data, so that the two datasets appear on a common scale centered at zero. Some of the apparent drawdown observed in the FTS total column measurements is due to systematic bias in the column at high SZA, and this illustrates the need to analyze the FTS column data symmetrically around local solar noon, as described in Section 3.6.3. Additionally, neglecting the transport term in Equation 3.6 introduces an error that varies between days.

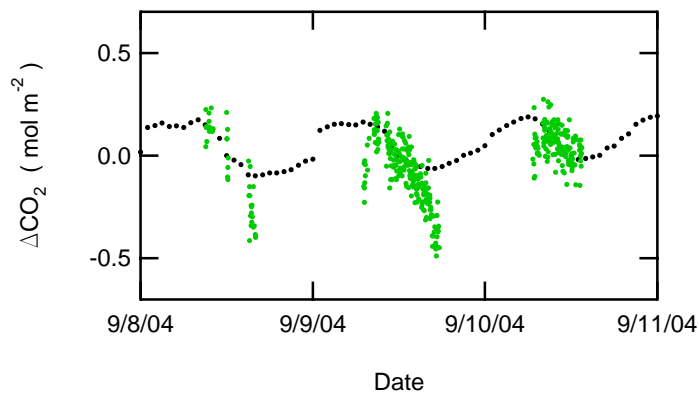


Figure 3.4. Comparison of the drawdown observed during 8 Sept – 11 Sept 2004 in the eddy covariance and FTS total column measurements. The FTS total column measurements corrected by the change in surface pressure (Equation 3.6) are shown in green. The eddy covariance measurements of NEE are shown in black. The noontime average has been subtracted from each 24-hour period of data so that the measurements appear on a common scale around zero. Some of the overestimation of drawdown observed in the column measurements is due to systematic bias in the column retrievals at high solar zenith angles.

NEE calculated from the column measurements according to Equation 3.6, and separately from the eddy covariance measurements is shown in Figures 3.5a and 3.5b. The change in CO_2 observed by the column measurements includes contributions from both NEE and transport. As mentioned previously, we have analyzed differences in column CO_2 symmetrically around local solar noon to minimize problems with SZA dependence of the

FTS column retrievals. Figure 3.5 shows the integrated change in column CO_2 relative to elapsed time around local solar noon (e.g. 4:00 represents the change from 2 hours before local noon to 2 hours after local noon). If we assume that the column and eddy covariance measurements have sufficiently similar footprints, then the difference between Figure 3.5a and 3.5b will give an estimation of the transport term, as seen in Figure 3.5c.

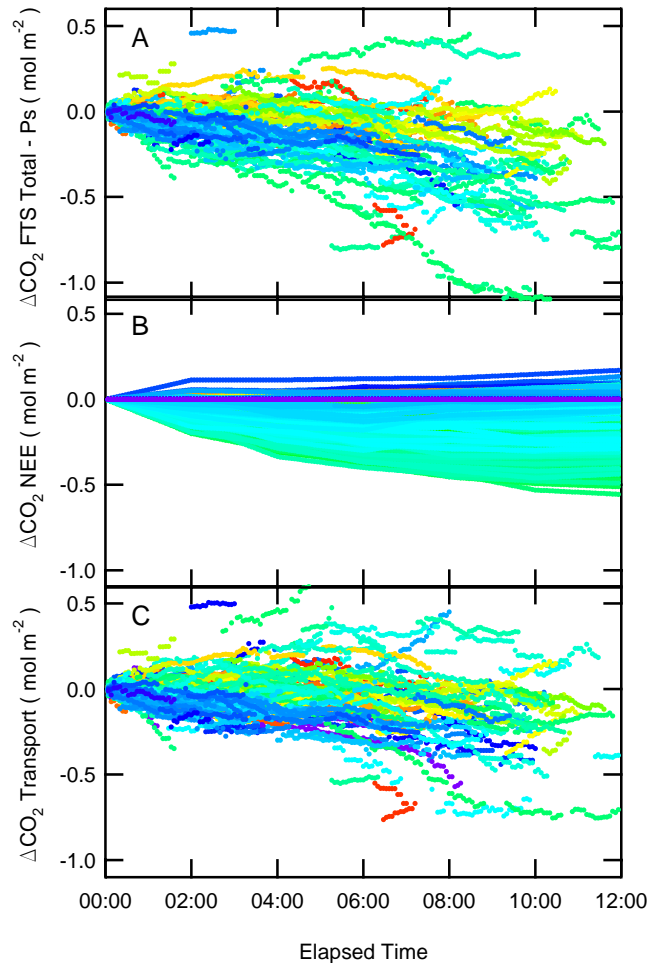


Figure 3.5. Comparison of NEE calculated from eddy covariance and column measurements. The elapsed time represents the time difference around local noon (e.g. 4:00 represents the change from 2 hours before local noon to 2 hours after local noon). Day of year is shown in color, with January as red and December as purple. (a) Change in column CO_2 observed by FTS measurements, calculated from Equation 3.6, including both NEE and transport. (b) Change in column CO_2 due to NEE, as measured by eddy covariance. (c) The difference between (a) and (b) is attributed to transport of air masses in the convective boundary layer and the free troposphere.

Figure 3.5c shows that, on average, the affect of transport is approximately neutral. Instead of quantifying the contribution of transport in Equation 3.6, we assume that it will introduce noise into our results, but will have no net contribution to the drawdown when averaged over several days.

With this assumption, we directly compare the drawdown observed in the FTS total column measurements and eddy covariance measurements during different seasons. The results are shown in Figure 3.6. The FTS total column measurements corrected by the change in surface pressure (Equation 3.6) and the eddy covariance measurements of NEE have been integrated over a four-hour period around local noon each day. As expected, Figure 3.6a shows significant variability in the drawdown observed by the FTS column measurements, due to the neglect of the transport term in Equation 3.6. However, when the data is averaged over seasonal timescales, the agreement is improved. This is consistent with the hypothesis that horizontal CO₂ gradients on average exert a neutral effect on the column. Because the column measurements are biased to sunny conditions, only coincident eddy covariance measurements of NEE are included in the seasonal average. The final panel of Figure 3.6 shows the correlation between column and eddy covariance measurements of CO₂ drawdown. The differences between the two techniques may represent differences in the measured footprint. Alternatively, if wind direction and regional CO₂ gradients are correlated seasonally, then the transport term may introduce a seasonal bias between the column and eddy covariance measurements of NEE.

These results show that the column measurements are sufficiently precise to observe CO₂ exchange. However, the results would be improved by better constraining changes in the CO₂ column due to transport.

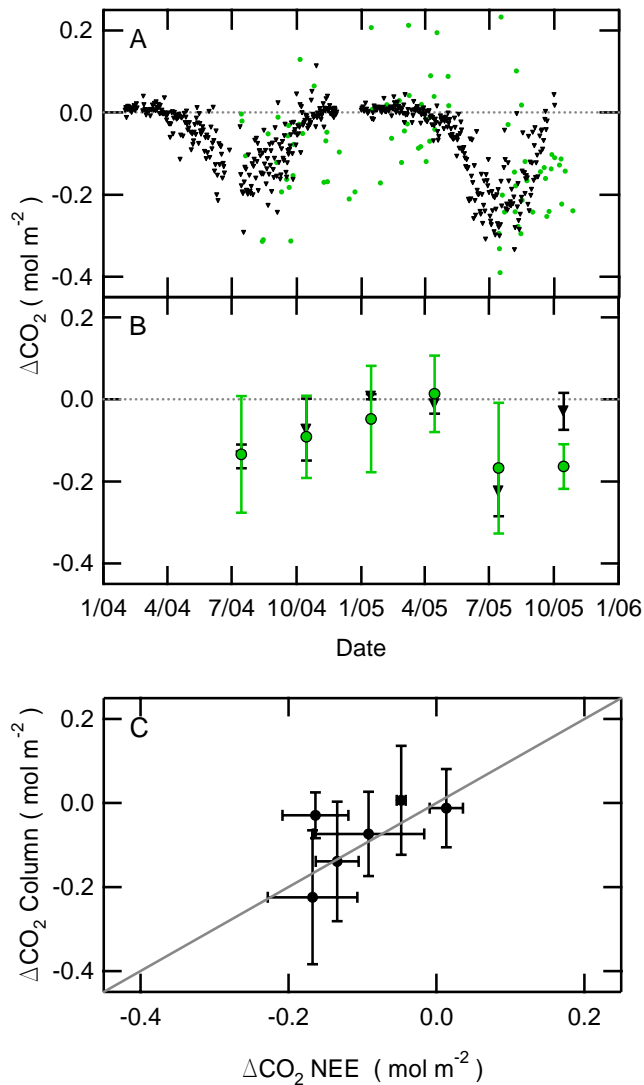


Figure 3.6. (a) Drawdown observed by eddy covariance and total column measurements during a four-hour period bracketing local solar noon. The FTS total column measurements corrected by the change in surface pressure (Equation 3.6) are shown in green. The eddy covariance measurements of NEE are shown in black. (b) Seasonal average of measurements shown in (a). Because the column measurements are biased to sunny conditions, only coincident eddy covariance measurements of NEE are included in the seasonal average. Error bars represent the $\pm 1\sigma$ standard deviation of the mean. (c) Correlation plot showing agreement between FTS total column measurements corrected by the change in surface pressure and eddy covariance measurements of NEE on seasonal timescales.

3.7 Conclusions

The initial Park Falls results presented here demonstrate how high-precision column measurements can yield information about carbon exchange. The observed peak-to-peak seasonal amplitude is 11 ± 1 ppmv during 2004 – 2006, with an observed secular increase

of 1.8 ppmv yr⁻¹. Comparison of column and surface measurements at the WLEF Tall Tower site is consistent with predictions that the column measurements represent the Northern Hemispheric average. Comparison of the column seasonal cycle with TransCom 3 models shows that the models underrepresent the amplitude of the seasonal cycle. This suggests that the CASA neutral biosphere model fluxes used in the TransCom 3 intercomparison may underpredict NEE. Finally, the column measurements have demonstrated potential for directly observing CO₂ exchange on local geographical scales, but this ability is limited by the difficulty in constraining atmospheric transport.

3.8 References

- Intergovernmental Panel on Climate Change (2001), *Climate Change 2001: The Scientific Basis*, Cambridge University Press, Cambridge.
- Bakwin, P. S., P. P. Tans, D. F. Hurst, and C. L. Zhao (1998), Measurements of carbon dioxide on very tall towers: results of the NOAA/CMDL program, *Tellus*, 50, 401-415.
- Baldocchi, D. D. (2003), Assessing the eddy covariance technique for evaluating carbon dioxide exchange rates of ecosystems: past, present and future, *Glob. Change Biol.*, 9, 479-492.
- Baldocchi, D. D., B. B. Hicks, and T. P. Meyers (1988), Measuring biosphere-atmosphere exchanges of biologically related gases with micrometeorological methods, *Ecology*, 69, 1331-1340.
- Battle, M., M. L. Bender, P. P. Tans, J. W. C. White, J. T. Ellis, T. Conway, and R. J. Francey (2000), Global carbon sinks and their variability inferred from atmospheric O₂ and δC¹³, *Science*, 287, 2467-2470.
- Berger, B. W., K. J. Davis, C. X. Yi, P. S. Bakwin, and C. L. Zhao (2001), Long-term carbon dioxide fluxes from a very tall tower in a northern forest: Flux measurement methodology, *J. Atmos. Ocean. Tech.*, 18, 529-542.
- Burrows, S. N., S. T. Gower, M. K. Clayton, D. S. Mackay, D. E. Ahl, J. M. Norman, and G. Diak (2002), Application of geostatistics to characterize leaf area index (LAI) from flux tower to landscape scales using a cyclic sampling design, *Ecosystems*, 5, 667-679.
- Conway, T. J., P. P. Tans, L. S. Waterman, and K. W. Thoning (1994), Evidence for interannual variability of the carbon cycle from the National Oceanic and Atmospheric

- Administration Climate Monitoring and Diagnostics Laboratory Global Air Sampling Network, *J. Geophys. Res.*, *99*, 22831-22855.
- Cook, B. D., K. J. Davis, W. G. Wang, A. Desai, B. W. Berger, R. M. Teclaw, J. G. Martin, P. V. Bolstad, P. S. Bakwin, C. X. Yi, and W. Heilman (2004), Carbon exchange and venting anomalies in an upland deciduous forest in Northern Wisconsin, USA, *Agr. Forest Meteorol.*, *126*, 271-295.
- Corbin, K. D., and A. S. Denning (2006), Using continuous data to estimate clear-sky errors in inversions of satellite CO₂ measurements, *Geophys. Res. Lett.*, *in press*.
- Dai, A., and J. H. Wang (1999), Diurnal and semidiurnal tides in global surface pressure fields, *J. Atmos. Sci.*, *56*, 3874-3891.
- Davis, K. J., P. S. Bakwin, C. X. Yi, B. W. Berger, C. L. Zhao, R. M. Teclaw, and J. G. Isebrands (2003), The annual cycles of CO₂ and H₂O exchange over a northern mixed forest as observed from a very tall tower, *Glob. Change Biol.*, *9*, 1278-1293.
- Denning, A. S., G. J. Collatz, C. G. Zhang, D. A. Randall, J. A. Berry, P. J. Sellers, G. D. Colello, and D. A. Dazlich (1996a), Simulations of terrestrial carbon metabolism and atmospheric CO₂ in a general circulation model: 1. Surface carbon fluxes, *Tellus*, *48*, 521-542.
- Denning, A. S., I. Y. Fung, and D. Randall (1995), Latitudinal gradient of atmospheric CO₂ due to seasonal exchange with land biota, *Nature*, *376*, 240-243.
- Denning, A. S., D. A. Randall, G. J. Collatz, and P. J. Sellers (1996b), Simulations of terrestrial carbon metabolism and atmospheric CO₂ in a general circulation model: 2. Simulated CO₂ concentrations, *Tellus*, *48*, 543-567.
- Dufour, E., F. M. Breon, and P. Peylin (2004), CO₂ column averaged mixing ratio from inversion of ground-based solar spectra, *J. Geophys. Res.*, *109*, doi:10.1029/2003JD004469.
- GLOBALVIEW-CO₂ (2005), GLOBALVIEW-CO₂: Cooperative Atmospheric Data Integration Project - Carbon Dioxide. CD-ROM, National Oceanic and Atmospheric Administration Climate Monitoring and Diagnostics Laboratory, Boulder, Colorado., edited.

- Goulden, M. L., J. W. Munger, S. M. Fan, B. C. Daube, and S. C. Wofsy (1996), Measurements of carbon sequestration by long-term eddy covariance: Methods and a critical evaluation of accuracy, *Glob. Change Biol.*, 2, 169-182.
- Gurney, K. R., R. M. Law, A. S. Denning, P. J. Rayner, D. Baker, P. Bousquet, L. Bruhwiler, Y. H. Chen, P. Ciais, S. Fan, I. Y. Fung, M. Gloor, M. Heimann, K. Higuchi, J. John, T. Maki, S. Maksyutov, K. Masarie, P. Peylin, M. Prather, B. C. Pak, J. Randerson, J. Sarmiento, S. Taguchi, T. Takahashi, and C. W. Yuen (2002), Towards robust regional estimates of CO₂ sources and sinks using atmospheric transport models, *Nature*, 415, 626-630.
- Gurney, K. R., R. M. Law, A. S. Denning, P. J. Rayner, D. Baker, P. Bousquet, L. Bruhwiler, Y. H. Chen, P. Ciais, S. M. Fan, I. Y. Fung, M. Gloor, M. Heimann, K. Higuchi, J. John, E. Kowalczyk, T. Maki, S. Maksyutov, P. Peylin, M. Prather, B. C. Pak, J. Sarmiento, S. Taguchi, T. Takahashi, and C. W. Yuen (2003), TransCom 3 CO₂ inversion intercomparison: 1. Annual mean control results and sensitivity to transport and prior flux information, *Tellus*, 55, 555-579.
- Houghton, R. A. (1999), The annual net flux of carbon to the atmosphere from changes in land use 1850-1990, *Tellus*, 51, 298-313.
- Keeling, C. D., T. P. Whorf, M. Wahlen, and J. Vanderpligt (1995), Interannual extremes in the rate of rise of atmospheric carbon dioxide since 1980, *Nature*, 375, 666-670.
- Keeling, R. F., R. P. Najjar, M. L. Bender, and P. P. Tans (1993), What atmospheric oxygen measurements can tell us about the global carbon cycle, *Global Biogeochem. Cy.*, 7, 37-67.
- Keeling, R. F., and S. R. Shertz (1992), Seasonal and interannual variations in atmospheric oxygen and implications for the global carbon cycle, *Nature*, 358, 723-727.
- MacKay, D. S., D. E. Ahl, B. E. Ewers, S. T. Gower, S. N. Burrows, S. Samanta, and K. J. Davis (2002), Effects of aggregated classifications of forest composition on estimates of evapotranspiration in a Northern Wisconsin forest, *Glob. Change Biol.*, 8, 1253-1265.
- Marland, G., T.A. Boden, and R.J. Andres (2000), Global, Regional, and National CO₂ Emissions, in Trends: A Compendium of Data on Global Change, edited, Carbon Dioxide Information Analysis Center, Oak Ridge National Laboratory, Oak Ridge.

- Olsen, S. C., and J. T. Randerson (2004), Differences between surface and column atmospheric CO₂ and implications for carbon cycle research, *J. Geophys. Res.*, *109*, doi:10.1029/2003JD003968.
- Randerson, J. T., M. V. Thompson, T. J. Conway, I. Y. Fung, and C. B. Field (1997), The contribution of terrestrial sources and sinks to trends in the seasonal cycle of atmospheric carbon dioxide, *Global Biogeochem. Cy.*, *11*, 535-560.
- Rayner, P. J., I. G. Enting, R. J. Francey, and R. Langenfelds (1999), Reconstructing the recent carbon cycle from atmospheric CO₂, δ¹³C and O₂/N₂ observations, *Tellus*, *51*, 213-232.
- Rayner, P. J., and D. M. O'Brien (2001), The utility of remotely sensed CO₂ concentration data in surface source inversions, *Geophys. Res. Lett.*, *28*, 175-178.
- Tans, P. P., I. Y. Fung, and T. Takahashi (1990), Observational constraints on the global atmospheric CO₂ budget, *Science*, *247*, 1431-1438.
- Wang, W. (2005), Regional estimates of net ecosystem-atmosphere exchange of carbon dioxide over a heterogeneous ecosystem, 235 pp, Pennsylvania State University.
- Wang, W. G., K. J. Davis, B. D. Cook, P. S. Bakwin, C. X. Yi, M. P. Butler, and D. A. Ricciuto (2005), Surface layer CO₂ budget and advective contributions to measurements of net ecosystem-atmosphere exchange of CO₂, *Agr. Forest Meteorol.*, *135*, 202-214.
- Warneke, T., Z. Yang, S. Olsen, S. Korner, J. Notholt, G. C. Toon, V. Velazco, A. Schulz, and O. Schrems (2005), Seasonal and latitudinal variations of column averaged volume-mixing ratios of atmospheric CO₂, *Geophys. Res. Lett.*, *32*, doi:10.1029/2004GL021597.
- Washenfelder, R. A., G. C. Toon, J.-F. Blavier, Z. Yang, N. T. Allen, P. O. Wennberg, S. A. Vay, D. M. Matross, and B. C. Daube (2006), Carbon dioxide column abundances at the Wisconsin Tall Tower site, *J. Geophys. Res.*, *in press*.
- WiDNR (1998), WISCLAND Land Cover (WLCGW930), Wisconsin Department of Natural Resources (WiDNR), Madison, Wisconsin.
- Wofsy, S. C., M. L. Goulden, J. W. Munger, S. M. Fan, P. S. Bakwin, B. C. Daube, S. L. Bassow, and F. A. Bazzaz (1993), Net exchange of CO₂ in a midlatitude forest, *Science*, *260*, 1314-1317.

- Yang, Z. H., G. C. Toon, J. S. Margolis, and P. O. Wennberg (2002), Atmospheric CO₂ retrieved from ground-based near IR solar spectra, *Geophys. Res. Lett.*, *29*, doi:10.1029/2001GL014537.
- Yi, C., K. J. Davis, P. S. Bakwin, B. W. Berger, and L. C. Marr (2000), Influence of advection on measurements of the net ecosystem-atmosphere exchange of CO₂ from a very tall tower, *J. Geophys. Res.*, *105*, 9991-9999.
- Zhao, C. L., P. S. Bakwin, and P. P. Tans (1997), A design for unattended monitoring of carbon dioxide on a very tall tower, *J. Atmos. Ocean. Tech.*, *14*, 1139-1145.

Chapter 4

TROPOSPHERIC METHANE RETRIEVED FROM GROUND-BASED NEAR-INFRARED SOLAR ABSORPTION SPECTRA*

*Adapted from R.A. Washenfelder, P.O. Wennberg, G.C. Toon (2003), *Geophysical Research Letters*, 30, doi: 10.1029/2003GL017969.

4.1 Abstract

High-resolution near-infrared solar absorption spectra recorded between 1977 and 1995 at the Kitt Peak National Solar Observatory are used to retrieve column abundances of methane (CH₄), hydrogen fluoride (HF), and oxygen (O₂). Employing a stratospheric "slope equilibrium" relationship between CH₄ and HF, the varying contribution of stratospheric CH₄ to the total column is inferred. Variations in the CH₄ column due to changes in surface pressure are determined from the O₂ column abundances. With this technique, CH₄ tropospheric volume mixing ratios are determined with a precision of ~0.5%. These display behavior similar to Mauna Loa in situ surface measurements, with a seasonal peak-to-peak amplitude of approximately 30 ppbv and a nearly linear increase between 1977 and 1983 of 18.0 ± 0.8 ppbv yr⁻¹, slowing significantly after 1990.

4.2 Introduction

Methane (CH₄), the most abundant hydrocarbon in the atmosphere, plays an important role in both radiative and chemical processes. Between 1984 and 1996, the globally-averaged CH₄ mole fraction increased from ~1625 to 1730 parts per billion by volume (ppbv) [Dlugokencky *et al.*, 1998]. Although the rate of increase is slowing, the cause of the variability has not been fully explained. Additional constraints on CH₄ sources and sinks are necessary to understand current behavior and to predict future trends.

Active in situ monitoring programs are in place, including those undertaken by the National Oceanic and Atmospheric Administration Climate Monitoring and Diagnostics Laboratory (NOAA CMDL) [Dlugokencky *et al.*, 1998] and the Global Atmospheric Gases

Experiment/Advanced Global Atmospheric Gases Experiment (GAGE/AGAGE) [Cunnold *et al.*, 2002]. Although these measurements are highly accurate, they have limited spatial coverage.

Space-based column measurements of CH₄ using scattered sunlight in the near-infrared (near-IR) have been proposed (e.g. SCIAMACHY and MOPITT) as a means of providing better spatial coverage. The near-IR region is a good candidate for space-based remote sensing because (i) it is near the peak of the solar Planck function; (ii) the column averaging kernels peak at the surface, facilitating identification of CH₄ sources and sinks; (iii) thermal emission from the atmosphere and instrument are negligible compared with reflected sunlight, simplifying calibration and radiative transfer calculations. Unfortunately, CH₄ spectroscopy is poorly characterized in this region and suffers from both missing weak lines and incomplete quantum assignments [Brown *et al.*, 1992]. In this letter, we examine solar absorption spectra from the Kitt Peak National Solar Observatory to determine the suitability of the 2ν₃ band centered at 6001 cm⁻¹ for remote sensing of tropospheric CH₄.

This analysis provides a long-term CH₄ column time series beginning in 1977. Sampling of CH₄ by the NOAA CMDL network did not begin until 1983 and GAGE/AGAGE network measurements were not initiated until 1985. Flask samples [e.g. Blake and Rowland, 1986; Khalil and Rasmussen, 1983] extend the record back to the mid-1970s. The scarcity of frequent, high-precision measurements between 1977 and 1983 makes the Kitt Peak dataset especially valuable.

4.3 Determination of Tropospheric CH₄

Column CH₄ exhibits variability driven by (i) changes in surface pressure, (ii) changes in the tropospheric CH₄ volume mixing ratio (VMR), and (iii) changes in the amount of stratospheric CH₄ due to changes in tropopause altitude. The CH₄ mole fraction decreases significantly in the stratosphere due to oxidation by O(¹D), OH, and Cl. A 30-ppbv change in tropospheric CH₄ or a 30-hPa change in tropopause altitude will each produce ~1.5% variation in the sea level CH₄ column. Thus, to accurately determine the tropospheric CH₄ VMR, it is necessary to correct for variations in both surface pressure and stratospheric contribution.

Analysis of the pressure-broadened lineshape is commonly used to gain altitude information for gases retrieved in the mid-IR. However, this method is not optimal for the near-IR Kitt Peak spectra. For a typical CH₄ line at 6000 cm⁻¹, the Doppler width exceeds the air-broadened width at ~14 km, preventing retrieval of stratospheric profile information. In addition, profile retrievals are limited by the spectral resolution of the available Kitt Peak measurements (typically $\delta\nu = 0.02$ cm⁻¹), knowledge of the instrument lineshape, and lack of accurate air-broadening parameters for the CH₄ 2ν₃ band.

In this analysis, we instead use simultaneous column measurements of HF to more accurately quantify stratospheric CH₄ variations. Previous studies have demonstrated that HF and CH₄ are inversely correlated in the stratosphere [Luo *et al.*, 1995]. As stratospheric air ages and CH₄ is oxidized, the photolysis of chlorofluorocarbons (CFC) initiates a chain of reactions, eventually yielding F atoms that react with H₂O and CH₄ to form HF in the stratosphere.

Provided that the relationship between the CH₄ and HF VMRs is sufficiently linear, the CH₄-HF slope in the stratosphere can be applied directly to correct the CH₄ total column for stratospheric variations. Mathematically, this argument is shown by:

$$(4.1) \quad CH_{4VMR} = a + b \times HF_{VMR}, \quad b = \frac{\partial(CH_{4VMR})}{\partial(HF_{VMR})}.$$

The integrated column is:

$$(4.2) \quad X_{column} = \int_0^{P_S} X_{VMR} dp$$

with pressure (p) in units of molecules cm^{-2} and P_s equal to surface pressure. Therefore, by substitution:

$$(4.3) \quad CH_{4 \text{ column}} = \int_0^{P_s} (a + b \times HF_{VMR}) dp = a \times P_s + b \times HF_{\text{column}} .$$

Since $HF_{VMR} = 0$ in the troposphere, parameter a in Equation 4.1 is equal to the tropospheric CH_4 VMR, assuming that CH_4 is well-mixed in the troposphere. Because the atmospheric O_2 VMR (0.2095) is highly constant, the relationship $\text{O}_2 \text{ column} = 0.2095 \times P_s$ can be used to eliminate P_s from Equation 4.3 yielding:

$$(4.4) \quad CH_{4 \text{ trop VMR}} = a = \frac{0.2095 \times (CH_{4 \text{ column}} - b HF_{\text{column}})}{\text{O}_2 \text{ column}} .$$

Equation 4.4 includes both the surface pressure correction using $\text{O}_2 \text{ column}$ and the stratospheric correction using HF_{column} . Dividing by $\text{O}_2 \text{ column}$ also removes possible systematic errors in the spectra, temperature profile, or calculated airmass that are common to CH_4 , HF , and O_2 . This Equation implicitly assumes that CH_4 and HF have similar averaging kernels in the stratosphere. We determine tropospheric CH_4 VMRs by simultaneously retrieving CH_4 , HF , and O_2 columns from the Kitt Peak solar spectra and by employing two additional datasets to determine the stratospheric CH_4 – HF relationship, b , and its time dependence.

4.4 The Kitt Peak Spectra

The spectra analyzed in this work have been described previously [Yang *et al.*, 2002]. The dataset includes more than 400 high-resolution near-IR solar absorption spectra ($\delta\nu = \sim 0.02 \text{ cm}^{-1}$) obtained with the 1-m Fourier transform spectrometer (FTS) at the McMath telescope complex of the Kitt Peak National Solar Observatory (31.9 N, 111.6 W, 2.09 km above sea

level) between 1977 and 1995. Each of these spectra include the $4000 - 8000 \text{ cm}^{-1}$ region necessary for the simultaneous retrieval of CH_4 , O_2 , and HF. Many of these observations were used by *Wallace and Livingston* [1990] to determine the column-averaged dry air VMR of CH_4 and CO_2 . Their work used equivalent widths to analyze 12 manifolds of the $2\nu_3 \text{ CH}_4$ ($\nu_0 = 6001 \text{ cm}^{-1}$) band and 14 lines of the O_2 $0-0 \ ^1\Delta_g - ^3\Sigma_g^-$ ($\nu_0 = 7882 \text{ cm}^{-1}$) band.

Here, we reanalyze the Kitt Peak solar spectra using an improved spectral retrieval algorithm with updated spectroscopic linelists for CH_4 , O_2 , H_2O , and solar absorption lines. We simultaneously fit the entire O_2 band (containing more than 200 significant lines), the CH_4 $2\nu_3$ P-branch (containing ten significant manifolds), and the strong HF R(1) (1-0) line at 4038.96 cm^{-1} .

4.5 Spectral Analysis and Retrievals

The line-by-line fitting algorithm used in this work (GFIT) was developed at the Jet Propulsion Laboratory (JPL) for the analysis of solar absorption spectra. The use of the GFIT algorithm, temperature profiles for Kitt Peak, O_2 spectral parameters, and solar linelist have been described previously [*Yang et al.*, 2002]. The atmospheric CH_4 and HF a priori VMR profiles are based on JPL MkIV measurements recorded during balloon flights from Ft. Sumner, New Mexico and Daggett, California (both at $\sim 34^\circ\text{N}$).

Spectral parameters for the HF R(1) (1-0) line are taken from the HITRAN database. Line position, intensity, and ground-state energy parameters for the CH_4 $2\nu_3$ manifolds [*Margolis*, 1988; *Margolis*, 1990] are taken from HITRAN, but different air-broadened widths are employed. Since measurements of $2\nu_3$ linewidths have never been reported these lines are assigned air-broadened widths in HITRAN based on measurements of the ν_2 and ν_4 CH_4 bands [*Brown et al.*, 1992]. When these parameters were used to fit laboratory and atmospheric spectra, however, the residuals showed that the assigned widths are systematically large. Additionally, CH_4 columns initially retrieved from the Kitt Peak spectra had unreasonably large, symmetric daily variations of about 6% that peaked at noon. In our retrieval of CH_4 , we have substituted broadening parameters from the ν_3 band as these are expected to be more closely related to the $2\nu_3$ band than the values assigned in HITRAN. (See appendix for a detailed discussion.) To further minimize the airmass

dependence of the analysis, we fit only the P-branch (5880 – 5996 cm^{-1}). These manifolds are weaker than the R- and Q-branch manifolds, making this region less susceptible to errors in linewidth. The retrieved tropospheric CH_4 VMR is observed to vary by about 1% between 1 and 10 airmasses.

Fits to the $2\nu_3$ P-branch include a full range of ground-state energies, so retrieved column CH_4 is only weakly dependent on the assumed temperature profile (0.01% K^{-1}). Considering O_2 and HF temperature sensitivities as well (0.02% K^{-1} and 0.26% K^{-1} respectively), a systematic error of 5 K at all levels within a temperature profile would change the retrieved tropospheric CH_4 VMR in Equation 4.4 by ~ 2 ppbv ($\sim 0.1\%$).

A spectral fitting example for the CH_4 $2\nu_3$ P-branch and the HF R(1) (1-0) line is shown in Figure 4.1. A fit to the O_2 0-0 $^1\Delta_g - ^3\Sigma_g^-$ band ($\nu_0 = 7882 \text{ cm}^{-1}$) has been shown previously in *Yang et al.* [2002]. The residuals (model-observed) are also illustrated in Figure 4.1. We have excluded from further analysis 32 observations (7.7%) that produce column errors greater than 3.0% for O_2 or CH_4 , as estimated from the spectral residuals. An additional 94 observations (22.7%) that produce column errors greater than 9.0% for HF have also been eliminated. The remaining 288 spectra typically have column errors of 1.4 – 2.8% for O_2 , 1.7 – 2.7% for CH_4 , and 3.5 – 6.7% for HF. The required HF precision is modest, as it is used as a linear correction with relatively small sensitivity. A 30 hPa change in tropopause pressure results in a $\sim 1.5\%$ change in the CH_4 column, while the HF column changes by $\sim 15\%$.

The retrieved slant column amounts were divided by the calculated airmasses to determine vertical column amounts. The airmass calculation includes the 226-m optical path inside the telescope [*Brown, private communication*] and the effects of refraction. The column-averaged CH_4 VMRs ($0.2095 \times \text{CH}_4 \text{ column} / \text{O}_2 \text{ column}$) without the HF correction described in Equation 4.4 are shown in Figure 4.2a.

Monthly average CH_4 flask data from NOAA CMDL's Mauna Loa site are also shown in Figure 4.2a. The dotted trend line through the May 1983 to 1995 data are the twelve-month

running average. The average seasonal cycle is determined by subtracting the running average from the data and binning the results by month. No evidence has been found for

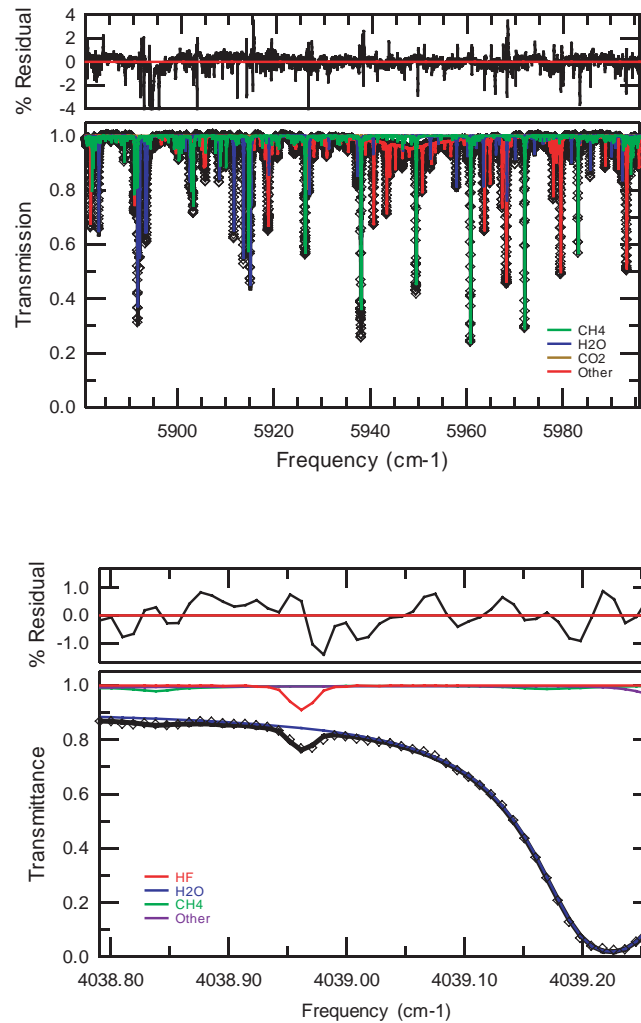


Figure 4.1 Example of a spectral fit to a Kitt Peak spectrum measured at 70.94° SZA on 9 May 1981, showing (a) the CH₄ 2v₃ P-branch at 5880 – 5996 cm⁻¹ and (b) the HF R(1) (1-0) line at 4038.9625 cm⁻¹. Diamonds are the measurements and black lines are the fitted transmittance. Contributions from individual gases are shown in color.

changes in the amplitude of the CH₄ seasonal cycle [Dlugokencky *et al.*, 1997], so this approximation is reasonable. The trend prior to May 1983, for which no Mauna Loa flask data is available, is a linear extrapolation with a slope that is consistent with the reported global tropospheric CH₄ increase of 18 ± 2 ppbv yr⁻¹ during 1978 to 1983 [Blake and

Rowland, 1986]. The average Mauna Loa seasonal cycle was then applied to the linear growth rate for 1977 to May 1983. The extrapolation of the seasonal cycle is used here only as a visual guide.

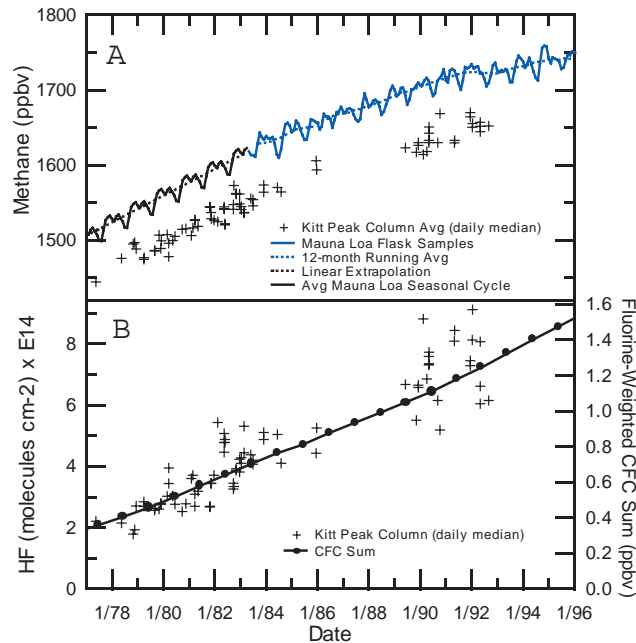


Figure 4.2 (a) Time series of Kitt Peak column-averaged CH_4 , determined from $0.2095 \times \text{CH}_4 \text{ column} / \text{O}_2 \text{ column}$. Mauna Loa flask samples (monthly average) are shown with their twelve-month running average. No Mauna Loa flask data exists prior to May 1983. A linear extrapolation with slope $18.0 \text{ ppbv yr}^{-1}$ is shown for this period, with the average Mauna Loa seasonal cycle applied. (b) Time series of Kitt Peak column HF. The fluorine-weighted CFC sum (CFC-11 + 2 \times CFC-12 + 3 \times CFC-113 + 2 \times HCFC-22) has been lagged by six years to account for atmospheric transport into the stratosphere.

The retrieved Kitt Peak column-average CH_4 VMRs are systematically lower (4%) than the Mauna Loa flask samples. Some of this difference is expected as the CH_4 VMR is lower in the stratosphere, but geographical differences and uncertainty in the absolute CH_4 linestrengths and widths preclude meaningful comparison of the column-average CH_4 VMRs.

4.6 Tropospheric CH_4 Volume Mixing Ratios

The column-average CH_4 VMRs in Figure 4.2a include significant variability driven by changes in tropopause altitude. This is illustrated by the anti-correlation of CH_4 in Figure

4.2a with retrieved HF columns in Figure 4.2b. In many years the HF column varies by as much as a factor of two between summer and winter. The seasonal variation in HF is superimposed on its increasing burden due to increasing CFC VMRs. Figure 4.2b shows the fluorine-weighted CFC trend ($\text{CFC-11} + 2 \times \text{CFC-12} + 3 \times \text{CFC-113} + 2 \times \text{HCFC-22}$) reconstructed from measurements by the ALE/GAGE/AGAGE network at Cape Grim, Tasmania. The fluorine-weighted CFC sum is lagged by six years to account for atmospheric transport within the stratosphere. Further details are given in the appendix.

To retrieve the tropospheric CH_4 VMR using Equation 4.4, the correlation of CH_4 with HF, b , is needed. This slope is determined here from two datasets. The Halogen Occultation Experiment (HALOE) instrument on the Upper Atmosphere Research Satellite (UARS) has been measuring CH_4 and HF simultaneously in solar occultations since 1991 using the gas filter correlation technique [Russell *et al.*, 1993]. The CH_4 -HF plots for that data are characterized by tightly fitted curves for different latitude bands [Luo *et al.*, 1995]. Using sunrise and sunset data measured at tangent latitudes of $20 - 40^\circ\text{N}$, we have fitted a linear CH_4 -HF relationship. The second CH_4 -HF dataset was recorded by the JPL MkIV Interferometer during 8 balloon flights at tangent latitudes between $32 - 38^\circ\text{N}$ during 1990 to 1996. The MkIV is an FTS that uses the solar occultation technique to record mid-IR spectra [Toon, 1991].

Figure 4.3 shows the slope of the CH_4 -HF correlation, b , obtained from the HALOE and

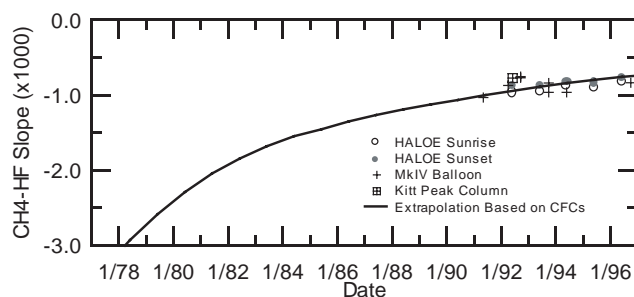


Figure 4.3 CH_4 -HF slope values, b , obtained from the HALOE, MkIV, and Kitt Peak data. Slope values have been extrapolated back to 1977 using the CFC sum shown in Figure 4.2b.

MkIV data for pressure levels between 10 and 100 hPa. The value calculated from the retrieved Kitt Peak CH_4 and HF columns is also shown. The CH_4 -HF slope has increased significantly between 1977 and 1995, due to increasing HF VMRs. The slope has been extrapolated back to 1977 using the time-lagged VMR of fluorine-weighted CFCs, shown in Figure 4.2b. Although this extrapolation is not ideal, it is necessary due to the lack of simultaneous CH_4 and HF profile measurements available from the 1970s and 1980s. Further explanation of the HALOE, MkIV, and Kitt Peak b values, as well as extrapolation of b using CFC data, is given in the appendix.

Tropospheric CH_4 VMRs calculated from Equation 4.4 are shown in Figure 4.4a. The Mauna Loa data in Figure 4.4a is identical to those in Figure 4.2a. The Kitt Peak

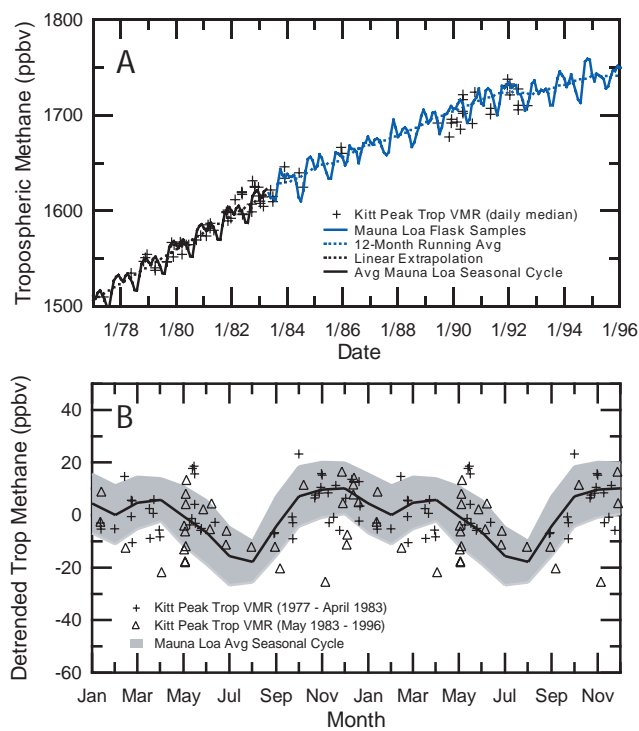


Figure 4.4 (a) Time series of Kitt Peak tropospheric CH_4 VMR, determined from Equation 4.4. The data have been multiplied by 1.015 (see text) to bring them into agreement with the Mauna Loa data. (b) Detrended Kitt Peak tropospheric CH_4 VMR shown together with the average Mauna Loa seasonal cycle (2σ variability). Kitt Peak data prior to May 1983 are represented by crosses and later data are represented by triangles.

tropospheric CH₄ VMRs are scaled by 1.015 to bring their values into agreement with the Mauna Loa data. This scaling was empirically determined to minimize bias between the Kitt Peak and Mauna Loa data. The linear slope of the 1977 to 1983 Kitt Peak tropospheric VMRs is 18.0 ± 0.8 ppbv yr⁻¹, consistent with the value of 18 ± 2 reported by *Blake and Rowland* [1986] for this period.

The average seasonal cycle (and 2σ variability) for the 1983 to 1995 Mauna Loa data is shown in Figure 4.4b. The Kitt Peak data were detrended by subtracting the linear trend and twelve-month running average shown in Figure 4.4a. Figure 4.4b shows that approximately $\pm 2\%$ seasonal variation is evident in the Kitt Peak data, consistent with the Mauna Loa data.

4.7 Conclusions

Reanalysis of the high-resolution near-IR spectra obtained at the Kitt Peak National Solar Observatory demonstrates that tropospheric CH₄ VMRs can be retrieved with 0.5% precision. However, our results are limited by current CH₄ spectroscopy (linewidths, intensities, and missing weak lines) and by our ability to accurately separate tropospheric and stratospheric variability using Equation 4.4. The largest errors in this analysis include noise in our HF retrievals, the assumption of a linear CH₄–HF relationship in the stratosphere, and the difficulty of extrapolating this relationship into the past. Despite these challenges, reanalysis of the Kitt Peak spectra allows the tropospheric CH₄ record to be extended back to 1977. These results show that high-precision measurements of column CH₄ are possible using ground-based FTS, and that this technique can be used to validate future space-based observations. However, to determine CH₄ sources and sinks from column measurements, it will be necessary to separate the tropospheric and stratospheric column contributions. This letter uses HF as a stratospheric tracer to achieve this separation. In the future, higher resolution spectra and precise laboratory measurements of air-broadened widths may allow direct retrieval of tropospheric CH₄ VMRs.

4.8 Acknowledgments

We thank the Kitt Peak personnel who acquired these spectra. We thank Linda Brown, Ming Luo, James Randerson, and Zhonghua Yang for helpful discussions. We acknowledge the NOAA CMDL and GAGE/AGAGE networks for the use of their data.

4.9 Appendix: Pressure Broadening of the CH₄ 2ν₃ Band

In HITRAN, the CH₄ 2ν₃ lines in the 5880 – 6110 cm⁻¹ region are assigned air-broadened half-widths based on their calculated lower-state energy. These values were taken from measurements of the ν₂ and ν₄ CH₄ bands [*Brown et al.*, 1992]. All CH₄ lines with the same lower-state energy were assigned the same width. When the HITRAN linelist is used to fit atmospheric spectra, the residuals suggest that the assigned widths are systematically high. This was confirmed by fitting the 2ν₃ region of a high-resolution laboratory spectrum obtained by Linda Brown at the Kitt Peak FTS that contained 5.3 hPa CH₄ in 785.7 hPa dry air.

Although no width measurements have been reported for the CH₄ 2ν₃ band, recent measurements report N₂, Ar, and O₂-broadened widths for the ν₃ Q-branch [*Pine*, 1992] and N₂ and Ar-broadened widths for the ν₃ P- and R-branches [*Pine*, 1997]. These are expected to be more closely related to the 2ν₃ band than the ν₂ and ν₄ values previously assigned in HITRAN. We calculated air-broadened half-widths for the ν₃ Q-branch by taking the weighted average of the N₂, O₂, and Ar widths (0.7808, 0.2095, and 0.0093 respectively). The ν₃ P- and R-branch air-broadened half-widths were found by scaling the reported N₂-broadened half-widths by 0.987 (the average ratio of air-broadened to N₂-broadened half-width in the ν₃ Q-branch).

The calculated ν₃ width values were then substituted directly for the corresponding (same branch, manifold, symmetry, and ordering index) 2ν₃ lines. The weaker, unidentified CH₄ lines in the 5880 – 6110 cm⁻¹ region belong to overtone and combination bands. For these lines, lower-state J values were calculated from the lower-state energies reported in HITRAN, according to $J_0 = -0.5 + 0.5 \times (1 + 0.769 \times E'')^{1/2}$. Average widths were calculated for each manifold of the ν₃ Q-branch reported by Pine [1992], and these were

substituted for the unidentified lines. All unidentified CH₄ lines with the same lower-state energy are assigned the same width. None of the self-broadened half-widths are changed.

4.10 Appendix: Correlation of HF and CH₄ in the Lower and Mid Stratosphere: the Determination of b(t)

As described in the main text, the stratospheric correlation between CH₄ and HF is determined using two datasets. The HALOE instrument on the UARS has been measuring CH₄ and HF simultaneously in solar occultations since 1991 using the gas filter correlation technique [Russell *et al.*, 1993]. The CH₄–HF correlation plots for this data are characterized by tightly-fitted curves for different latitude bands [Luo *et al.*, 1995]. Although the relationship in high northern latitudes is nearly linear, Luo *et al.* conclude that CH₄ and HF are not in a state of perfect "slope equilibrium." In particular, the data indicate slightly different slopes above and below ~6 hPa (where CH₄ ~1.0 ppm). After examining the CH₄–HF correlations for 20 – 40 °N tangent latitudes in the publicly available Version 19 data, we conclude that, for 10 – 100-hPa levels of relevance to this work, the HALOE data is sufficiently linear (Figure 4.5a). There is a small offset between CH₄–HF slopes determined from sunrise and sunset occultations, resulting from a systematic measurement error reported during HALOE validation [Park *et al.*, 1996; Russell *et al.*, 1996].

The second CH₄–HF dataset was recorded by the JPL MkIV Interferometer during 8 balloon flights at tangent latitudes between 32 - 38 °N during 1990 to 1996. The MkIV is a Fourier transform infrared spectrometer that uses the solar occultation technique to record mid-IR spectra [Toon, 1991]. MkIV measurements of the stratospheric fluorine budget have been reported previously [Sen *et al.*, 1996]. We determined simultaneous HF and CH₄ VMR profiles from three strong HF lines at 3877.7071, 4038.9621 and 4109.9359 cm⁻¹, and 39 microwindows containing unblended CH₄ lines in the mid-IR between 1225 - 4630 cm⁻¹. Although the 3877.7071 and 4109.9359 cm⁻¹ lines are obscured by strong water absorptions in the ground-based Kitt Peak spectra, these lines are well-resolved in the MkIV balloon measurements. For the CH₄–HF correlation, data obtained for tangent pressures between 10 and 100 hPa were used. CH₄–HF slopes from the MkIV data are shown in Figure 4.5b.

We also determined the CH₄–HF relationship for the Kitt Peak data. For this analysis, we verified that the CH₄ and HF averaging kernels are similar in the stratosphere (Figure 4.6).

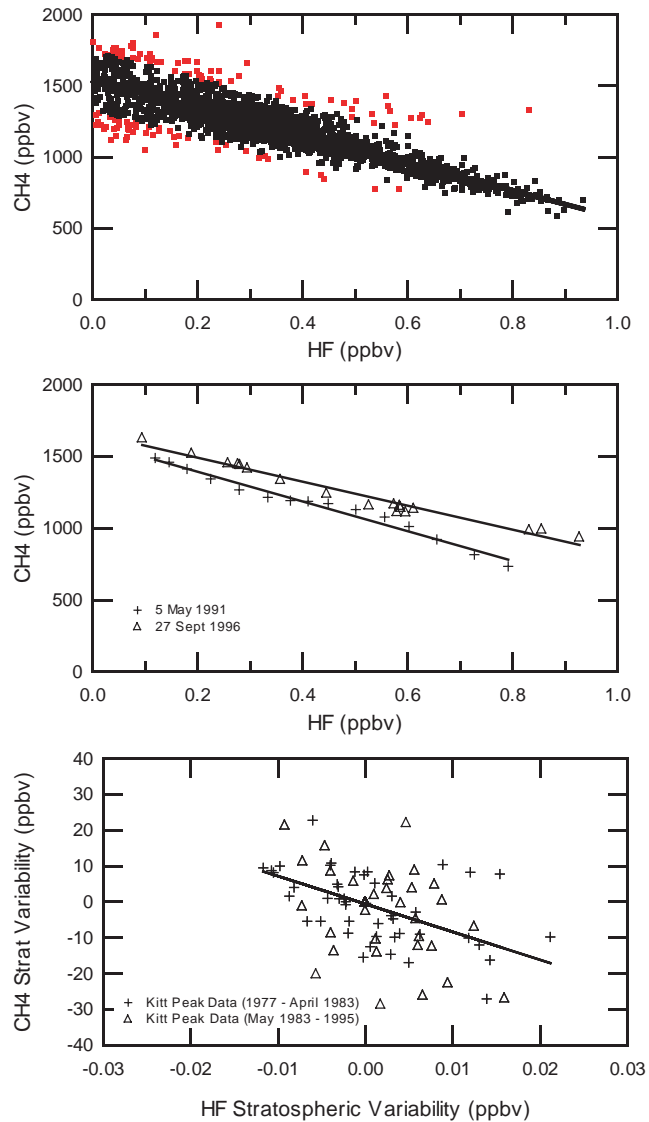


Figure 4.5 (a) CH₄ and HF data (Version 19) from the HALOE instrument on UARS during 1992 sunrise occultations recorded at 20 – 40°N and 10 – 100 hPa. Two sigma outliers shown in red. (b) CH₄ and HF data recorded between 10 – 100 hPa by the MkIV balloon interferometer during two flights. A total of 8 solar occultations at 32 – 38°N were analyzed, but for clarity only two are shown here. (c) Relationship between stratospheric column-average CH₄ and HF. Kitt Peak column-average CH₄ was detrended by Mauna Loa flask sample data. Kitt Peak column-average HF was detrended by the fluorine-weighted CFC sum lagged by six years. Linear-least squares slope is -7.8×10^2 with $r^2 = 0.19$.

Demonstrating correlation between the stratospheric component of retrieved Kitt Peak CH₄ and HF shows that the tropospheric and stratospheric components can be separated. In order to plot the stratospheric CH₄–HF correlation for the Kitt Peak data covering many years, it is necessary to subtract the tropospheric trend from the CH₄ data and the

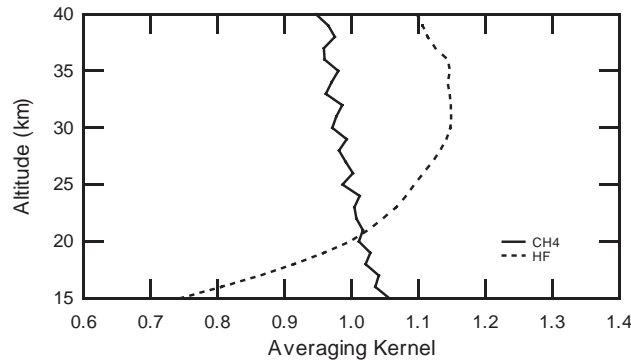


Figure 4.6 CH₄ and HF averaging kernels for a Kitt Peak spectrum measured at 70.94° SZA on 9 May 1981.

stratospheric trend from the HF data. The stratospheric CH₄ component is calculated as the retrieved Kitt Peak values shown in Figure 4.2a minus the Mauna Loa values, with both datasets normalized by their respective means. Since the column-average measurement of CH₄ is heavily weighted in the troposphere, no time lag is applied between the Mauna Loa observations and the Kitt Peak column-averages.

All of the short-term HF variation observed is due to changes in tropopause altitude. However, the interpretation is still difficult because CFC VMRs increased substantially between 1977 and 1995. We determined the fluorine trend from CFC-11, CFC-12, CFC-113, and HCFC-22 measurements and reconstructed histories from the ALE/GAGE/AGAGE network at Cape Grim, Tasmania [McCulloch *et al.*, 2003; Miller *et al.*, 1998; Walker *et al.*, 2000]. The total HF trend is equal to the fluorine-weighted sum of the CFCs: CFC-11 + 2 × CFC-12 + 3 × CFC-113 + 2 × HCFC-22. Together, these gases accounted for 94.6% of the stratospheric fluorine loading during the early 1990s [(IPCC), 2001]. The fluorine-weighted CFC sum is lagged by six years to account for atmospheric transport within the stratosphere. This is consistent with HALOE measurements of HF at

54 - 56 km [Considine *et al.*, 1999]. The time lagged fluorine-weighted CFC sum is shown in Figure 4b. The HF variation due strictly to stratospheric change was determined from (HF scaled by mean - lagged CFC sum scaled by mean) / (CFC scaled by mean).

The resulting plot of stratospheric CH₄ vs. HF for the Kitt Peak dataset is shown in Figure 4.5c. The -7.8×10^2 slope of this dataset is consistent with the HALOE and MkIV slopes. The coefficient of determinant, r^2 , is 0.19. Although the Kitt Peak correlation alone is insufficient to justify a CH₄-HF slope correction, its agreement with the HALOE and MkIV data provides support for using Equation 4.4 to calculate tropospheric CH₄ VMRs. MkIV and HALOE data are only available for 1991 - present. Changing CFC VMRs in the past will cause the CH₄-HF slope to vary. We have extrapolated the CH₄-HF slope, $b(t)$, from 1991 to 1977 by $b(t) = b(1992) / \text{fluorine-weighted CFC sum}(t - 6 \text{ years})$, with the fluorine-weighted CFC sum normalized to 1 in 1992.

4.11 References

- Intergovernmental Panel on Climate Change (2001), *Climate Change 2001: The Scientific Basis*, Cambridge University Press, Cambridge.
- Blake, D. R., and F. S. Rowland (1986), Worldwide increase in tropospheric methane, 1978-1983, *J. Atmos. Chem.*, *4*, 43-62.
- Brown, L. R., J. S. Margolis, J. P. Champion, J. C. Hilico, J. M. Jouvard, M. Loete, C. Chackerian, G. Tarrago, and D. C. Benner (1992), Methane and its isotopes - Current status and prospects for improvement, *J. Quant. Spectrosc. Radiat. Transfer*, *48*, 617-628.
- Considine, G. D., L. E. Deaver, E. E. Remsberg, and J. M. Russell (1999), Analysis of near-global trends and variability in Halogen Occultation Experiment HF and HCl data in the middle atmosphere, *J. Geophys. Res.*, *104*, 24297-24308.
- Cunnold, D. M., L. P. Steele, P. J. Fraser, P. G. Simmonds, R. G. Prinn, R. F. Weiss, L. W. Porter, S. O'Doherty, R. L. Langenfelds, P. B. Krummel, H. J. Wang, L. Emmons, X. X. Tie, and E. J. Dlugokencky (2002), In situ measurements of atmospheric methane at GAGE/AGAGE sites during 1985-2000 and resulting source inferences, *J. Geophys. Res.*, *107*, doi:10.1029/2001JD001226.

- Dlugokencky, E. J., K. A. Masarie, P. M. Lang, and P. P. Tans (1998), Continuing decline in the growth rate of the atmospheric methane burden, *Nature*, *393*, 447-450.
- Dlugokencky, E. J., K. A. Masarie, P. P. Tans, T. J. Conway, and X. Xiong (1997), Is the amplitude of the methane seasonal cycle changing?, *Atmos. Environ.*, *31*, 21-26.
- GLOBALVIEW-CO2 (2005), GLOBALVIEW-CO2: Cooperative Atmospheric Data Integration Project - Carbon Dioxide. CD-ROM, National Oceanic and Atmospheric Administration Climate Monitoring and Diagnostics Laboratory, Boulder, Colorado., edited.
- Khalil, M. A. K., and R. A. Rasmussen (1983), Sources, sinks, and seasonal cycles of atmospheric methane, *J. Geophys. Res.*, *88*, 5131-5144.
- Luo, M., R. J. Cicerone, and J. M. Russell (1995), Analysis of Halogen Occultation Experiment HF Versus CH₄ correlation plots - Chemistry and transport implications, *J. Geophys. Res.*, *100*, 13927-13937.
- Margolis, J. S. (1988), Measured line positions and strengths of methane between 5500 and 6180 cm⁻¹, *Appl. Opt.*, *27*, 4038-4051.
- Margolis, J. S. (1990), Empirical values of the ground-state energies for methane transitions between 5500 and 6150 cm⁻¹, *Appl. Opt.*, *29*, 2295-2302.
- McCulloch, A., P. M. Midgley, and P. Ashford (2003), Releases of refrigerant gases (CFC-12, HCFC-22 and HFC-134a) to the atmosphere, *Atmos. Environ.*, *37*, 889-902.
- Miller, B. R., J. Huang, R. F. Weiss, R. G. Prinn, and P. J. Fraser (1998), Atmospheric trend and lifetime of chlorodifluoromethane (HCFC-22) and the global tropospheric OH concentration, *J. Geophys. Res.*, *103*, 13237-13248.
- Park, J. H., J. M. Russell, L. L. Gordley, S. R. Drayson, D. C. Benner, J. M. McInerney, M. R. Gunson, G. C. Toon, B. Sen, J. F. Blavier, C. R. Webster, E. C. Zipf, P. Erdman, U. Schmidt, and C. Schiller (1996), Validation of Halogen Occultation Experiment CH₄ measurements from the UARS, *J. Geophys. Res.*, *101*, 10183-10203.
- Pine, A. S. (1992), Self-Broadening, N₂-broadening, O₂-broadening, H₂-broadening, Ar-broadening, and He-broadening in the ν_3 band Q-branch of CH₄, *J. Chem. Phys.*, *97*, 773-785.
- Pine, A. S. (1997), N₂ and Ar broadening and line mixing in the P and R branches of the ν_3 band of CH₄, *J. Quant. Spectrosc. Radiat. Transfer*, *57*, 157-176.

- Russell, J. M., L. E. Deaver, M. Z. Luo, R. J. Cicerone, J. H. Park, L. L. Gordley, G. C. Toon, M. R. Gunson, W. A. Traub, D. G. Johnson, K. W. Jucks, R. Zander, and I. G. Nolt (1996), Validation of hydrogen fluoride measurements made by the Halogen Occultation Experiment from the UARS platform, *J. Geophys. Res.*, *101*, 10163-10174.
- Russell, J. M., L. L. Gordley, J. H. Park, S. R. Drayson, W. D. Hesketh, R. J. Cicerone, A. F. Tuck, J. E. Frederick, J. E. Harries, and P. J. Crutzen (1993), The Halogen Occultation Experiment, *J. Geophys. Res.*, *98*, 10777-10797.
- Sen, B., G. C. Toon, J. F. Blavier, E. L. Fleming, and C. H. Jackman (1996), Balloon-borne observations of midlatitude fluorine abundance, *J. Geophys. Res.*, *101*, 9045-9054.
- Toon, G. C. (1991), The Jet Propulsion Laboratory MkIV Interferometer, *Opt. Photonics News*, *2*, 19-21.
- Walker, S. J., R. F. Weiss, and P. K. Salameh (2000), Reconstructed histories of the annual mean atmospheric mole fractions for the halocarbons CFC-11, CFC-12, CFC-113, and carbon tetrachloride, *J. Geophys. Res.*, *105*, 14285-14296.
- Wallace, L., and W. Livingston (1990), Spectroscopic observations of atmospheric trace gases over Kitt Peak: 1. Carbon dioxide and methane from 1979 to 1985, *J. Geophys. Res.*, *95*, 9823-9827.
- Yang, Z. H., G. C. Toon, J. S. Margolis, and P. O. Wennberg (2002), Atmospheric CO₂ retrieved from ground-based near IR solar spectra, *Geophys. Res. Lett.*, *29*, doi:10.1029/2001GL014537.